Nucleic Acids Research, 2022 **1**
https://doi.org/10.1093/nar/gkac1060

SirA inhibits the essential DnaA:DnaD interaction to block helicase recruitment during *Bacillus subtilis* sporulation

Charles Winterhalter [1], Daniel Stevens[1], Stepan Fenyk[1], Simone Pelliciari[1], Elie Marchand[2], Panos Soultanas [3], Aravindan Ilangovan[4] and Heath Murray [1,*]

[1]Centre for Bacterial Cell Biology, Biosciences Institute, Newcastle University, Newcastle Upon Tyne NE2 4AX, UK, [2]Research Unit in Biology of Microorganisms, Department of Biology, Université de Namur, Namur, Belgium, [3]Biodiscovery Institute, School of Chemistry, University of Nottingham, Nottingham NG7 2RD, UK and [4]Blizard Institute, School of Biological and Behavioural Sciences, Queen Mary University of London, Newark street, London E1 2AT, UK

Received April 19, 2022; Revised October 04, 2022; Editorial Decision October 22, 2022; Accepted October 24, 2022

ABSTRACT

Bidirectional DNA replication from a chromosome origin requires the asymmetric loading of two helicases, one for each replisome. Our understanding of the molecular mechanisms underpinning helicase loading at bacterial chromosome origins is incomplete. Here we report both positive and negative mechanisms for directing helicase recruitment in the model organism *Bacillus subtilis*. Systematic characterization of the essential initiation protein DnaD revealed distinct protein interfaces required for homo-oligomerization, interaction with the master initiator protein DnaA, and interaction with the helicase co-loader protein DnaB. Informed by these properties of DnaD, we went on to find that the developmentally expressed repressor of DNA replication initiation, SirA, blocks the interaction between DnaD and DnaA, thereby restricting helicase recruitment from the origin during sporulation to inhibit further initiation events. These results advance our understanding of the mechanisms underpinning DNA replication initiation in *B. subtilis*, as well as guiding the search for essential cellular activities to target for antimicrobial drug design.

INTRODUCTION

Genome replication initiates at specific chromosomal loci termed origins. Throughout the domains of life, initiator proteins containing a conserved AAA+ (*A*TPase *A*ssociated with various cellular *A*ctivities) motif assemble at chromosome origins and direct loading of two helicases for the onset of DNA replication (1). Interestingly, while the initiation pathway in both bacteria and eukaryotes culminates in a ring shaped hexameric helicase encircling a single DNA strand, the molecular mechanisms necessary to achieve this crucial helicase loading step appear to be distinct (2). Bacteria use their master initiator DnaA to unwind the chromosome origin (*oriC*) and then to help load helicases around ssDNA such that they are poised to start unwinding (3,4). The eukaryotic initiator ORC (*O*rigin *R*ecognition *C*omplex) also promotes helicase loading, but in this case the annular enzyme is deposited around double-stranded DNA (dsDNA) in a dormant state which must subsequently be activated to form an open complex and encircle a single strand (5,6). These distinctions make bacterial DNA replication initiation proteins attractive targets for the development of novel antibiotics (7–9).

Despite decades of study, the molecular mechanisms coordinating helicase recruitment and loading at *oriC* during the bacterial cell cycle are yet to be fully understood (2,10–12). Moreover, bacteria are not known to extrinsically regulate helicase recruitment. Instead, regulatory factors are thought to target the dsDNA binding and oligomerisation activities of DnaA to influence chromosome origin binding and unwinding (13,14).

DnaA is a multifunctional enzyme composed of four distinct domains that act in concert during DNA replication initiation (Supplementary Figure S1A) (15). Domain IV contains a helix-turn-helix dsDNA binding motif and a basic loop with a conserved arginine that specifically recognizes a 9 bp asymmetric sequence called the 'DnaA-box' (consensus 5′-TTATCCACA-3′) (16–18). Domain III is composed of the AAA+ motif that can assemble into an ATP-dependent right-handed helical oligomer (19–21). Domain III also contains residues required for a

*To whom correspondence should be addressed. Tel: +44 191 208 3233; Fax: +44 191 208 7424; Email: heath.murray@newcastle.ac.uk
Present address: Elie Marchand, Research Unit in Biology of Microorganisms, Department of Biology, Université de Namur, Namur, Belgium.

DnaA oligomer to interact specifically with a trinucleotide ssDNA binding element termed the 'DnaA-trio' (consensus 3′-GAT-5′) (22–24). It has been proposed that a DnaA oligomer, guided by DnaA-boxes and DnaA-trios within *oriC*, interacts with one strand of the DNA duplex to promote chromosome origin opening (22,24–26).

DnaA domain II tethers domains III/IV to domain I, which acts as an interaction hub. Domain I ($DnaA^{DI}$) facilitates homo-oligomerization, either directly through self-interaction (27) or indirectly via accessory proteins such as DiaA and HobA (28,29). Domain I also interacts with important regulatory proteins such as HU, Dps and SirA (30–33) and has weak affinity for ssDNA (34). However, the most important role of $DnaA^{DI}$ is thought to be recruiting the replicative helicase. This may occur either directly, as for *Escherichia coli* DnaA (35,36) or indirectly, as for *B. subtilis* DnaA (Figure 1A) (37,38). Interestingly, in both cases the same surface of DnaA domain I is suggested to be involved (Supplementary Figure S1B, C) (34,37,39–41).

In *B. subtilis,* along with DnaA, the essential DnaD and DnaB proteins are required for recruiting the DnaC:DnaI complex (helicase and AAA+ chaperone, respectively) to the chromosome origin. Enrichment of initiation proteins at *oriC* has been shown to follow a linear pathway (Figure 1A) (38,42,43). While DnaD and DnaB are required during both replication initiation and restart at repaired replication forks (44), a mechanistic understanding of the activities performed by these replication proteins has remained elusive (37,38,45,46).

In this paper we focus on DnaD. DnaD has three functional regions: N-terminal domain ($DnaD^{NTD}$), C-terminal domain ($DnaD^{CTD}$) and C-terminal tail ($DnaD^{CTT}$) (Figure 1C). The crystal structure of $DnaD^{NTD}$ revealed a homodimer with a large interface stabilizing the two monomers (47). At low concentrations the $DnaD^{NTD}$ was found to be a tetramer in solution (48), hence a model of the DnaD dimer:dimer interface was proposed based on the observed symmetry of $DnaD^{NTD}$ dimers packed within the crystal (47). Furthermore, it has been suggested that the prominent winged-helix motif within the $DnaD^{NTD}$ might act as a scaffold for the formation of higher order oligomeric species (42). However, the $DnaD^{CTD}$ structure was solved as a monomer (43) and the functional significance of DnaD oligomerization *in vivo* was unknown.

The DnaD protein:protein interactions required for *B. subtilis* DNA replication initiation have yet to be clearly defined. An interaction with DnaA was proposed to involve residues located in both the $DnaD^{NTD}$ (Phe51, Ile83, Glu95) and the $DnaD^{CTD}$ (Ile132, Glu134, Glu169, Val171) (37,40), while an interaction with DnaB was suggested to involve the $DnaD^{NTD}$ (37,43). Critically however, the functional significance of specific DnaD interactions with DnaA and DnaB *in vivo* was unclear.

To explore the role of *B. subtilis* DnaD in the mechanism of DNA replication initiation, we performed a systematic alanine scan to identify residues essential for DnaD activities within its physiological environment of a cell. Structural and functional characterization of DnaD identified residues required for homo-oligomerization (Phe6, Leu22) and for protein:protein interactions with DnaA (Phe51, Pro54, Ile83, Ile92, Glu95) and DnaB (Trp229). Guided by these discoveries, we went on to find that the developmentally expressed regulator of DNA replication initiation, SirA, blocks the interaction of DnaA with DnaD, thus inhibiting helicase recruitment during the early stages of sporulation to impede further rounds of DNA replication. Conservation of DnaD in several bacterial pathogens suggests that the DnaA:DnaD interface is an attractive target for rational drug design.

MATERIALS AND METHODS

Reagents

Nutrient agar (NA; Oxoid) was used for routine selection and maintenance of both *B. subtilis* and *E. coli* strains. Supplements were added as required: ampicillin (100 μg/ml), chloramphenicol (5 μg/ml), kanamycin (5 μg/ml), spectinomycin (50 μg/ml in *B. subtilis*, 100 μg/ml in *E. coli*), tetracycline (10 μg/ml), erythromycin (1 μg/ml) in conjunction with lincomycin (25 μg/ml), X-gal (0.01% v/v), xylose (0.35% v/v), IPTG (0.1 mM unless indicated otherwise). All chemicals and reagents were obtained from Sigma-Aldrich unless otherwise noted. Antibodies were purchased from Eurogentec. Plasmid extractions were performed using Qiagen miniprep kits. Other reagents used for specific techniques are listed within the method details.

Biological resources: *B. subtilis* strains

B. subtilis strains are listed in Supplementary Table S1 and were propagated at 37°C in Luria-Bertani (LB) medium unless stated otherwise in method details. Transformation of competent *B. subtilis* cells was performed using an optimized two-step starvation procedure as previously described (49,50). Briefly, recipient strains were grown overnight at 37°C in transformation medium (Spizizen salts supplemented with 1 μg/ml Fe-NH_4-citrate, 6 mM $MgSO_4$, 0.5% w/v glucose, 0.02 mg/ml tryptophan and 0.02% w/v casein hydrolysate) supplemented with IPTG where required. Overnight cultures were diluted 1:17 into fresh transformation medium supplemented with IPTG where required and grown at 37°C for 3 h with continual shaking. An equal volume of prewarmed starvation medium (Spizizen salts supplemented with 6 mM $MgSO_4$ and 0.5% w/v glucose) was added and the culture was incubated at 37°C for 2 h with continuous shaking. DNA was added to 350 μl cells and the mixture was incubated at 37°C for 1 h with continual shaking. 20–200 μl of each transformation was plated onto selective media supplemented with IPTG where required and incubated at 37°C for 24–48 h. The genotype of all chromosomal *dnaA* and *dnaD* mutants was confirmed by DNA sequencing. Descriptions, where necessary, are provided below.

CW197 [*trpC2* Δ*dnaD amyE*::*spc*(P_{HAT}-*dnaD-ssrA lacI*$^{Q18M/W220F}$)] was constructed to study potentially lethal mutants of *dnaD in vivo* (Figure 1B). First, an ectopic copy of *dnaD* was placed under the control of an IPTG-inducible promoter ($P_{HYPERSPANK}$) (51). When combined with a deletion mutant of the native *dnaD*, the basal expression level of the ectopic copy was sufficient to sustain growth. Two approaches were taken to reduce the basal expression of the ectopic *dnaD*, lowering promoter activity and reducing

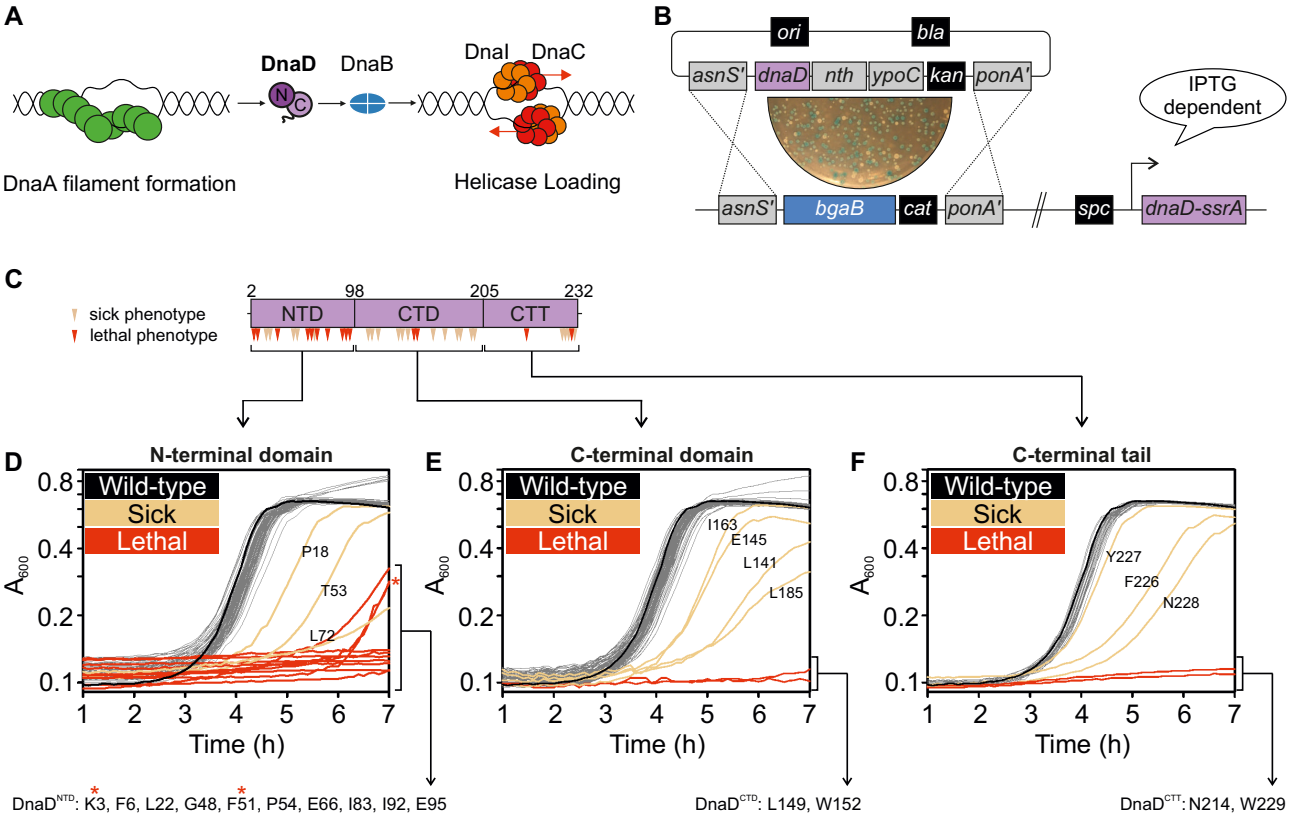

Figure 1. Identification of essential residues in *B. subtilis* DnaD. (**A**) Schematics of the helicase loading pathway in *B. subtilis* showing sequential recruitment of DnaA, DnaD, DnaB and the helicase complex DnaI-DnaC. For DnaD schematics, N and C indicate N-/C-terminal domains respectively. (**B**) DnaD blue/white screening assay. An integration vector carrying individual *dnaD* substitutions is integrated by double homologous recombination at the *dnaD* locus. Plasmid variants were constructed from pCW66. The recipient strain (CW197) is kept alive by the induction of the ectopic *dnaD-ssrA* with IPTG and selection of white colonies following transformation of *dnaD* substitutions is performed in the presence of kanamycin, the chromogenic substrate X-Gal and IPTG. (**C**) DnaD primary structure mapped with substitutions that conferred a phenotype. Residues are marked as red for lethal and beige for altered growth (translucent/heterogeneous phenotype or slow growth). NTD denotes the N-Terminal Domain, CTD the C-Terminal Domain and CTT the C-Terminal Tail of DnaD. (**D–F**) Plate reader growth assays of DnaD variants located within the protein N-terminal domain (D), C-terminal domain (E) or C-terminal tail (F) in the absence of DnaD-ssrA. The black line shows the growth profile of cells harbouring wild-type *dnaD*, whereas beige lines highlight slow-growing variants and red line lethal substitutions. Note that some lethal substitutions develop suppressor mutations that activate the expression of *dnaD-ssrA* (red star). Lists of the DnaD variants that revealed a lethal phenotype by growth in plate reader assays are provided below panels (D-F): K3 (CW289). F6 (CW310), L22 (CW292), G48 (CW293), F51 (CW174), P54 (CW295), E66 (CW311), I83 (CW170), I92 (CW297), E95 (CW166), L149 (CW308), W152 (CW302), N214 (CW283), W229 (CW286). All strains in (D, E) are referenced in Supplementary Table S6, the wild-type control is CW162 and the parent strain of all DnaD mutants is CW197.

DnaD stability. Promoter activity was inhibited by altering the transcription start site from A to T (P_{HAT}) and introducing mutations into *lacI* (Q18M/W220F) that increase operator binding (Supplementary Figure S2A) (52,53). DnaD stability was reduced by fusing the ectopic *dnaD* to an *ssrA* degradation tag (AANDENYSENYALGG) (54). Together these modifications produced a suitable expression system that conditionally complements the *dnaD* deletion mutant only when the ectopic *dnaD-ssrA* is induced (Supplementary Figure S2B). Immunoblot analysis confirmed nearly complete degradation of DnaD-ssrA following removal of IPTG within 30 min (Supplementary Figure S2C).

CW252 [*trpC2 amyE::spec(lacI* $P_{HYPERSPANK}$*-sirA) ganA::erm(xylR* P_{XYL}*-dnaD)*] was constructed by transformation with a PCR product generated by three-way Gibson assembly (NEBuilder HiFi). The *dnaD* gene with its native ribosome binding site was amplified using oCW611 and oCW612 with 168CA genomic DNA as template. The flanking region containing *ganA′-xylR-*P_{XYL} was amplified using oCW284 and oCW614 with pJMP1 as template. The flanking region containing *erm-′ganA* was amplified using oCW613 and oCW130 with pJMP1 as template.

CW270/279/280 [*trpC2 amyE::spec(lacI* $P_{HYPERSPANK}$*-sirA) ganA::erm(xylR* P_{XYL}*-dnaD***)* with * being I83A, F51A and E95A were constructed identically to CW252 with the exception of $dnaD^{F51A}$, $dnaD^{I83A}$ and $dnaD^{E95A}$ being amplified using oCW611 and oCW612 from CW174, CW170 and CW166 genomic DNA, respectively as templates.

DnaD alanine substitution strains were generated by a blue/white screening assay using CW197 as parental strain and mutant plasmids obtained after Quickchange mutagenesis and sequencing as recombinant DNA (Supplementary Figure S3). X-gal 0.016% w/v was added to transformation plates for detection of β-galactosidase activity and selection

of kanamycin resistant white colonies that integrated mutant DNA by double homologous recombination. Three individual white colonies per mutant were then streaked onto a medium either with or without IPTG to identify alleles of interest.

Biological resources: *E. coli* strains and plasmids

E. coli transformations were performed in CW198 via heat-shock following the Hanahan method (55) for plasmids harbouring *dnaD* and propagated in LB with appropriate antibiotics at 37°C unless indicated otherwise in method details. Plasmids are listed in the Supplementary Table S2 (sequences are available upon request). DH5α [F^- Φ80*lac*ZΔM15 Δ(*lac*ZYA-*arg*F) U169 *rec*A1 *end*A1 *hsd*R17(r_k^-, m_k^+) *pho*A *sup*E44 *thi*-1 *gyr*A96 *rel*A1 λ^-] (56) was used for other plasmids construction. HM1784 [BTH101 *Δrnh*::*kan*] was used for bacterial-2-hybrid experiments and constructed by P1 transduction of *Δrnh*::*kan* from JW0204 (Keio collection) into BTH101 [F-, *cya-99*, *ara*D139, *gal*E15, *gal*K16, *rps*L1 (*Str*^{r}), *hsd*R2, *mcr*A1, *mcr*B1 (Euromedex)]. Descriptions, where necessary, are provided below.

pCW123, pCW141, pCW142, pCW143, pCW153, pCW163, pCW214, pHM543, pHM544, pHM545 were generated by Quickchange mutagenesis using the oligonucleotides listed in Supplementary Table S3.

pCW4 was generated by cloning *HindIII–SphI* PCR fragments generated using oligonucleotides listed in Supplementary Table S3.

pDS84, pDS119, pDS120, pDS126, pDS127, pDS132, pHM359, pHM638, pHM640, pHM642, pHM644 were generated by cloning *Asp718I-BamHI* PCR fragments generated using the oligonucleotides listed in Supplementary Table S3.

pCW66, pCW137, pCW171, pCW213, pSP75, pSP80, pSP81, pSP82, pSP83, pSP85 were generated by ligase-free cloning via two-step assembly processes using oligonucleotides listed in Supplementary Table S3. The underlined part of each primer indicates the region used to form an overlap. FastCloning (57) was used with minor modifications. PCR products (15 μl from a 50 μl reaction) were mixed and then subjected to a heating/cooling regime: two cycles of 98°C for 2 min then 25°C for 2 min, then one cycle of 98°C for 2 min then 25°C for 60 min. After cooling *DpnI* restriction enzyme (1 μl) was added to digest parental plasmids and the mixtures were incubated at 37°C for ∼4 h. Following digestion 10 μl of the PCR mixture was transformed into chemically competent *E. coli*. Where several primer pairs are listed for the construction of a single plasmid (Multi-step assembly column in Supplementary Table S3), multiple rounds of ligase free cloning were performed to obtain the final constructs.

DnaD alanine-scan mutant plasmids were generated by Quickchange mutagenesis using oligonucleotides listed in Supplementary Table S4. Cloning protocols were adapted to a 96-well plate format for PCR amplification of mutant plasmids, heat-shock and transformation recovery. All plasmids were sequenced.

Biological resources: oligonucleotides

All oligonucleotides were purchased from Eurogentec. Oligonucleotides used for plasmid construction are listed in Supplementary Table S3, those generated by the Quickchange program are listed in Supplementary Table S4 and oligonucleotides used for qPCR are listed in Supplementary Table S5. Details about the design of the Quickchange mutagenesis software can be found below.

Quickchange mutagenesis was used for the construction of the DnaD mutant plasmid library. Each point mutant was assembled by PCR using mutagenic primers carrying a single alanine substitution (58). We generated all mutant primer pairs via an in-house Quickchange program that optimised sequences according to key features in site-directed mutagenesis primer design (59). These include sequence length adjustments based on: (i) the melting temperature (T_M) of the oligonucleotide part that anneals to the template plasmid, (ii) the T_M corresponding to a primer pair overlapping section, (iii) the GC-content within different sections of individual primers, (iv) the presence of a GC-clamp at every oligonucleotide 3'-end, and (v) the T_M difference between forward and reverse primer pairs. Code was written in Java and is available online.

Statistical analyses

Statistical analysis was performed using Student's t-tests and *P*-values are given in figure legends. The exact value of *n* is given in method details and represents the number of biological repeats for an experiment. Tests were based on the mean of individual biological replicates and error bars indicate the standard error of the mean (SEM) across these measurements. Differences were considered as significant if their associated *P*-value was <0.05. For sporulation experiments showing protein depletion from the origin, the standard error of the mean was propagated by addition of the error from individual terms.

Data availability: new software

All original code to generate the QuickChange program has been deposited at Zenodo and is publicly available as of the date of publication. The DOI of the software is 10.5281/zenodo.5541537.

Microscopy

To visualize cells by microscopy during the exponential growth phase, starter cultures were grown in imaging medium (Spizizen minimal medium supplemented with 0.001 mg/ml ferric ammonium citrate, 6 mM magnesium sulphate, 0.1 mM calcium chloride, 0.13 mM manganese sulphate, 0.1% (w/v) glutamate, 0.02 mg/ml tryptophan) with 0.5% (v/v) glycerol, 0.2% (w/v) casein hydrolysate and 0.1 mM IPTG at 37°C. Saturated cultures were diluted 1:100 into fresh imaging medium supplemented with 0.5% (v/v) glycerol and 0.1 mM IPTG and allowed to grow for three mass doublings. For DnaD mutants, early log cells were then spun down for 5 min at 9000 rpm, resuspended in the same medium lacking IPTG and further incubated

for 90 min before imaging. For sporulation experiments, cells were grown in sporulation salts (60,61) and imaged throughout the course of sporulation.

Cells were mounted on ∼1.4% (w/v) agar pads (in sterile ultrapure water) and a 0.13- to 0.17-mm glass coverslip (VWR) was placed on top. Microscopy was performed on an inverted epifluorescence microscope (Nikon Ti) fitted with a Plan Apochromat Objective (Nikon DM 100×/1.40 Oil Ph3). Light was transmitted from a CoolLED pE-300 lamp through a liquid light guide (Sutter Instruments), and images were collected using a Prime CMOS camera (Photometrics). The fluorescence filter sets were from Chroma: GFP (49002, EX470/40 (EM), DM495lpxr (BS), EM525/50 (EM)), mCherry (49008, EX560/40 (EM), DM585lprx (BS), EM630/75 (EM)) and DAPI (49000, EX350/50, DM400lp, EM460/50). Digital images were acquired using METAMORPH software (version 7.7) and analysed using Fiji software (62). All experiments were independently performed at least twice, and representative data are shown.

Numbers of origins or GFP-DnaN foci were quantified using the Trackmate plugin within the Fiji software (63). Background was subtracted from fluorescence images set to detect 6–10 pixel blob diameter foci over an intensity threshold identical between images acquired on the same day. A mask containing the detected origin foci was created and merged with the nucleoids or membrane dye channels, and the number of origins per nucleoid was determined and averaged for a minimum of 100 cells from each strain that was examined. This analysis was performed for at least two individual biological repeats.

Phenotype analysis of *dnaD* mutants using the inducible *dnaD-ssrA* strain

Strains were grown for 18 h at 37°C on NA plates unless otherwise stated (spot-titre assays) or in Penassay Broth (PAB, plate reader experiments) either with or without IPTG (0.1 mM). All experiments were independently performed at least twice and representative data are shown.

Immunoblot analysis

Proteins were separated by electrophoresis using a NuPAGE 4–12% Bis–Tris gradient gel run in MES buffer (Life Technologies) and transferred to a Hybond-P PVDF membrane (GE Healthcare) using a semi-dry apparatus (Bio-rad Trans-Blot Turbo). DnaA, DnaD and FtsZ were probed with polyclonal primary antibodies (Eurogentec) and then detected with an anti-rabbit horseradish peroxidase-linked secondary antibody (A6154, Sigma) using an ImageQuant LAS 4000 mini digital imaging system (GE Healthcare). Detection of DnaA, DnaD and FtsZ was within a linear range. Experiments were independently performed at least twice and representative data are shown.

Protein structure representations

Protein representations were generated using the Pymol Molecular Graphics 2.1 software (64).

Bacterial two-hybrid assays

E. coli strain HM1784 was transformed using a combination of complementary plasmids and grown to an A_{600} of 0.5 in LB containing ampicillin and spectinomycin, before diluting 1:10 000 and spotting onto nutrient agar plates containing antibiotics and the indicator X-gal (0.008% w/v). Plates were incubated at 30°C for 24–48 h and imaged using a digital camera. Experiments were independently performed at least twice and representative data are shown.

Protein purification

Wild-type *dnaA* and *dnaD* were amplified by PCR using genomic DNA from *B. subtilis* 168CA and respectively cloned into pSF14 and pSF17 containing a His^{14}-SUMO tag. DnaD mutants were created from pSF17 via quickchange reactions to introduce single or multiple substitutions. Plasmids were propagated in *E. coli* DH5α and transformed in BL21(DE3)-pLysS for expression. Strains were grown in LB medium at 37°C. Overnight cultures were diluted 1:100 the next morning and at A_{600} of 0.6, 1 mM IPTG was added before further incubation at 30°C for 4 h. Cells were harvested by centrifugation at 7000 × g for 20 min, DnaA pellets resuspended in 40 ml of DnaA Ni^{2+} Binding Buffer (30 mM HEPES [pH 7.6], 250 mM potassium glutamate, 10 mM magnesium acetate, 30 mM imidazole), DnaD pellets resuspended in 40 ml of DnaD Ni^{2+} Binding Buffer (40 mM Tris–HCl [pH 8.0], 0.5 M NaCl, 5% w/v glycerol, 1 mM EDTA, 20 mM imidazole), each containing 1 EDTA-free protease inhibitor tablet (Roche #37378900) and then flash frozen in liquid nitrogen. Cell pellet suspensions were thawed and incubated with 0.5 mg/ml lysozyme on ice for 1 h before disruption by sonication (1 h at 20 W with 20 s pulse/rest intervals). Cell debris was removed from the lysate by centrifugation at 24 000 × g for 30 min at 4°C, then passed through a 0.2 μm filter for clarification. Further purification steps were performed at 4°C using a FPLC with a flow rate of 1 ml/min.

Clarified lysates were applied to a 1 ml HisTrap HP column (Cytiva). For DnaA, an additional wash with 10 ml Ni^{2+} High Salt Wash Buffer (30 mM HEPES [pH 7.6], 1 M potassium glutamate, 10 mM magnesium acetate, 30 mM imidazole) was performed. Materials bound to the column were washed with 10 ml of 10% Ni^{2+} Elution Buffer (DnaA: 30 mM HEPES [pH 7.6], 250 mM potassium glutamate, 10 mM magnesium acetate, 1 M imidazole; DnaD: 40 mM Tris–HCl [pH 8.0], 0.5 M NaCl, 1 mM EDTA, 0.5 M imidazole) and proteins were eluted with a 10 ml linear gradient (10–100%) of Ni^{2+} Elution Buffer. For DnaA, fractions containing the protein were applied to a 1 ml HiTrap Heparin HP affinity column (Cytiva) equilibrated in H Binding Buffer (30 mM HEPES [pH 7.6], 100 mM potassium glutamate, 10 mM magnesium acetate) and elution was carried out with a 20 ml linear gradient (20–100%) of H Elution Buffer (30 mM HEPES [pH 7.6], 1 M potassium glutamate, 10 mM magnesium acetate). Fractions containing proteins of interest were pooled and digested with 10 μl of 10 mg/ml His^{14}-Tev-SUMO protease (65). For DnaD, digestion was performed at room temperature over the course of 48 h and the same amount of His^{14}-Tev-SUMO protease was added after 24 h digestion.

Digestion reactions were applied to a 1 ml HisTrap HP column to capture non-cleaved monomers, His^{14}-SUMO tag and His^{14}-TEV-SUMO protease. Cleaved proteins were collected in the flow-through and their purity was confirmed using SDS-PAGE. Glycerol was added (DnaA: 20% v/v final; DnaD: 10% v/v final) and proteins aliquots were flash frozen in liquid nitrogen before being stored at –80°C.

SEC-MALS

Experiments were conducted on a system comprising a Wyatt HELEOS-II multi-angle light scattering detector and a Wyatt rEX refractive index detector linked to a Shimadzu HPLC system (SPD-20A UV detector, LC20-AD isocratic pump system, DGU-20A3 degasser and SIL-20A autosampler) and the assays performed at 20°C. Solvent was 0.2 μm filtered before use and a further 0.1 μm filter was present in the flow path. The column was equilibrated with at least 2 column volumes of 40 mM Tris–HCl [pH 8], 500 mM NaCl, 1 mM EDTA, 20 mM imidazole, 2.5% (v/v) glycerol before use and flow was continued at the working flow rate until baselines for UV, light scattering and refractive index detectors were all stable.

The sample injection volume was of 100 μl, the Shimadzu LabSolutions software was used to control the HPLC and the Astra 7 software for the HELEOS-II and rEX detectors. The Astra data collection was 1 min shorter than the LC solutions run to maintain synchronisation. Blank buffer injections were used as appropriate to check for carry-over between sample runs. Data were analysed using the Astra 7 software. Molecular weights were estimated using the Zimm fit method with degree 1 and a value of 0.179 was used for protein refractive index increment (dn/dc).

Oligomerization crosslinking assay

Protein concentrations were adjusted to 300 nM in 1.2× Conjugation Buffer (20 mM HEPES [pH 7.2], 100 mM NaCl, 10 mM magnesium acetate) and 15 μl reactions were allowed to equilibrate at 20°C. BS_3 (ThermoFisher A39266) was used as a crosslinking agent and diluted in water to a stock concentration of 750 μM. For final concentrations of 250 nM protein and 500× molar excess BS_3, 3 μl of crosslinker was gently mixed with protein reactions. All reactions were incubated for 6 min at 20°C, then stopped by adding Quenching Buffer (final concentration 50 mM Tris–HCl [pH 7.5]) and further incubated for 10 min. NuPAGE loading dye (ThermoFisher NP0007) supplemented with excess DTT was added to all reactions and samples were fixed for 5 min at 95°C before loading on a 4–12% Bis-Tris gel (Invitrogen WG1402BOX). The same samples without BS_3 were run as a loading control and stained using a coomassie protein stain (Abcam ab119211) because detection via our anti-DnaD antibody (Eurogentec) varied between wild-type and mutant alleles of *dnaD*. After migration, species were transferred to a Hybond-P PVDF membrane (GE Healthcare) using a semi-dry apparatus (Bio-rad Trans-Blot Turbo). Proteins were probed via α-DnaD polyclonal primary antibodies (Eurogentec) and then detected with an anti-rabbit horseradish peroxidase-linked secondary antibody (A6154, Sigma) using an ImageQuant LAS 4000 mini digital imaging system (GE Healthcare). Experiments were independently performed at least twice and representative data is shown.

Sequence alignments

Multiple protein sequence alignments were performed using the Clustal Omega tool (66). Protein sequences are listed in Supplementary Table S7.

Phenotype analysis of *dnaA* mutants using the inducible *oriN* strain

Strains were grown for 48 h at 30, 37 or 48°C on NA plates either with or without IPTG (0.1 mM). All experiments were independently performed at least twice and representative data is shown.

DNA strand separation assay

DNA scaffolds that contained one oligonucleotide labelled with BHQ2, one with Cy5 and one unlabelled (12.5 nM final concentration) were diluted in 10 mM HEPES–KOH [pH 8], 100 mM potassium glutamate, 2 mM magnesium acetate, 30% glycerol, 10% DMSO and 1 mM nucleotide (ADP or ATP). All the reactions were prepared on ice to ensure the stability of the DNA probe, then allowed to equilibrate at 20°C. DnaA was added to a final concentration of 650 nM to allow displacement of all the probes. Reactions were performed using a flat-bottom black polystyrene 96-well plate (Costar #CLS3694) in triplicate and fluorescence was detected every minute over 60 min with a plate reader (BMG Clariostar). For all reactions a negative control without protein was used as background. At each timepoint the average background value was subtracted from the experimental value, thus reporting the specific DnaA activity on a single substrate. Error bars indicate the standard error of the mean over three biological replicates.

ChIP

Chromatin immunoprecipitation was performed as previously described (67) with minor modifications detailed below. Strains were grown overnight at 30°C in Spizizen salts supplemented with tryptophan (20 μg/ml), glutamate (0.1% w/v), glucose (0.5% w/v) and casamino acid (0.2% w/v). The following day cultures were diluted 1:100 into fresh medium and allowed to grow to an A_{600} of 0.4. Samples were resuspended in PBS and cross-linked with formaldehyde (final concentration 1% v/v) for 10 min at room temperature, then quenched with 0.1 M glycine. Cells were pelleted at 4°C, washed three times with ice-cold PBS (pH 7.3) then frozen in liquid nitrogen and stored at –80°C. Frozen cell pellets were resuspended in 500 μl of lysis buffer (50 mM NaCl, 10 mM Tris–HCl [pH 8.0], 20% w/v sucrose, 10 mM EDTA, 100 μg/ml RNase A, $\frac{1}{4}$ complete mini protease inhibitor tablet (Roche), 2000 K U/μl Ready-Lyse lysozyme (Epicentre)) and incubated at 37°C for 30 min to degrade the cell wall. 500 μl of immunoprecipitation buffer (300 mM NaCl, 100 mM Tris–HCl [pH 7.0], 2% v/v Triton X-100, $\frac{1}{4}$ complete mini protease inhibitor tablet (Roche),

1 mM EDTA) was added to lyse the cells and the mixture was incubated at 37°C for a further 10 min before cooling on ice for 5 min. DNA samples were sonicated (40 amp) three times for 2 min at 4°C to obtain an average fragment size of ∼500–1000 bp. Cell debris was removed by centrifugation at 4°C and the supernatant transferred to a fresh Eppendorf tube. To determine the relative amount of DNA immunoprecipitated compared to the total amount of DNA, 100 μl of supernatant was removed, treated with Pronase (0.5 mg/ml) for 60 min at 37°C then stored on ice. To immunoprecipate protein-DNA complexes, 800 μl of the remaining supernatant was incubated with rabbit polyclonal anti-DnaA, anti-DnaD and anti-DnaB antibodies (Eurogentec) for 1 hour at room temperature. Protein-G Dynabeads (750 μg, Invitrogen) were equilibrated by washing with bead buffer (100 mM Na_3PO_4, 0.01% v/v Tween 20), resuspended in 50 μl of bead buffer, and then incubated with the sample supernatant for 1 h at room temperature. The immunoprecipated complexes were collected by applying the mixture to a magnet and washed with the following buffers for 15 min in the respective order: once in 0.5× immunoprecipitation buffer; twice in 0.5× immunoprecipitation buffer + NaCl (500 mM); once in stringent wash buffer (250 mM LiCl, 10 mM Tris–HCl [pH 8.0], 0.5% v/v Tergitol-type NP-40, 0.5% w/v sodium deoxycholate 10 mM EDTA). Finally, protein-DNA complexes were washed a further three times with TET buffer (10 mM Tris–HCl [pH 8.0], 1 mM EDTA, 0.01% v/v Tween 20) and resuspended in 100 μl of TE buffer (10 mM Tris–HCl [pH 8.0], 1 mM EDTA). Formaldehyde crosslinked complexes for both the immunoprecipate and total DNA were reversed by incubation at 65°C for 16 h in the presence of 1000 U Proteinase K. DNA was then removed from the magnetic beads, cleaned using QIAquick PCR Purification columns (Qiagen) and used for qPCR analysis.

Marker frequency analysis

Strains were grown in PAB overnight at 37°C and diluted 1:100 the next morning in PAB. Cells were allowed to grow for 4 h at 37°C or incubated until they reached an optical density of 0.4 for cold-sensitive assays performed at 20°C. Five hundred microliter samples were harvested and immediately mixed with sodium azide (1% w/v final) to arrest growth and genome replication. Cultures were collected by centrifugation, the supernatant was discarded and pellets were flash frozen in liquid nitrogen before gDNA extraction via the DNeasy blood and tissue kit (Qiagen).

Real-time quantitative PCR (qPCR)

qPCR was performed using the Luna qPCR mix (NEB) to measure the amount of genomic loci bound to DnaA, DnaD and DnaB. PCR reactions (overall volume 20 μl in a Rotor-Disc 100, Qiagen) were run in a Rotor-Gene Q Instrument (Qiagen) using serial dilutions of the immunoprecipitate and total DNA as templates. Oligonucleotide primers designed to amplify *oriC* (qSF11/qSF12), *oriN* (qSF5/qSF6) and the non-specific locus *yhaX* (oWKS145/oWKS146 (45)) were typically 20–25 bases in length and amplified a ∼100 bp PCR product (Supplementary Table S5). Standard curves were performed using Rotor-Gene Q Software v2.0.2 (Qiagen) to calculate the efficiency of each PCR reaction, which varied ∼5% between primer pairs. Following qPCR reactions, a melt curve analysis was performed to confirm the specificity of each product. For ChIP experiments, individual enrichment values were obtained in two steps. First, every Cq value was normalised to $1/2^{cq}$, the dilution factor used during the qPCR, and technical triplicates were averaged to a single value. Second, for each primer pair the relative %IP was obtained by normalising to the amount of total DNA in the sample. For marker frequency analysis, the $^{ori}/_{Ter}$ ratio of each sample was normalized to the $^{ori}/_{Ter}$ ratio of a DNA sample from *B. subtilis* spores in which contain a single chromosome ($^{ori}/_{Ter} = 1$). Error bars indicate the standard error of the mean for 3–8 biological replicates.

Pull-down assay of His_6-$DnaA^{DI}$-$DnaD^{NTD}$ complexes

BL21 (DE3) *E. coli* cells containing the different expression plasmids (pSP75, pSP80, pSP81, pSP82, pSP83 and pSP85) were grown overnight in 5 ml of LB supplemented with kanamycin at 37°C. The following day cells were diluted in 50 ml of fresh medium until A_{600} reached 0.5. Protein expression was induced by adding 1 mM IPTG for 4 h at 30°C. Cells were collected by centrifugation and resuspended in 2 ml of resuspension buffer (30 mM Hepes [pH 7.5], 250 mM potassium glutamate, 10 mM magnesium acetate, 20% w/v sucrose, 30 mM imidazole) supplemented with 1 EDTA-free protease inhibitor tablet. Bacteria were lysed with two sonication cycles at 10 W for 3 min with 2 s pulses. Cell debris was pelleted by centrifugation at 25 000 × g at 4°C for 30 min and the supernatant was passed through a 0.2 μm filter. The clarified lysate was then loaded onto Ni-NTA spin columns (QIAgen) and proteins purified according to manufacturer protocol washing the column with Washing Buffer (30 mM HEPES [pH 7.5], 250 mM potassium glutamate, 10 mM magnesium acetate, 20% sucrose, 100 mM imidazole) and eluting bound proteins with elution buffer (30 mM HEPES [pH 7.5], 250 mM potassium glutamate, 10 mM magnesium acetate, 20% w/v sucrose, 1 M imidazole). The eluates were loaded on a NuPAGE 4–12% Bis–Tris gradient gel run in MES buffer (Life Technologies) and analysed with IstantBlue staining (Merck).

RESULTS

DnaD is an essential DNA replication initiation protein in the model organism *B. subtilis* and in opportunistic human pathogens such as *Staphylococcus aureus* and *Streptococcus pneumoniae* (68–70). However, the specific activities required by DnaD at the chromosome origin *in vivo* are unclear. To address these questions, we sought to identify essential amino acids in *B. subtilis* DnaD and then to determine the function of each essential residue.

Identification of essential residues in DnaD

Functional analysis of bacterial DNA replication initiation proteins *in vivo* is challenging because they are required for viability. Mutation of an essential feature will be lethal,

while mutations that severely disable function can result in the rapid accumulation of compensatory suppressors. To circumvent these issues, a bespoke inducible complementation system was developed for *dnaD* (P_{HAT}-*dnaD-ssrA*, Supplementary Figure S2). Upon repression of the ectopic *dnaD-ssrA*, the functionality of *dnaD* alleles at the endogenous locus can be determined.

A plasmid for allelic exchange of the endogenous *dnaD* gene was created (Supplementary Figure S3). Using this template, a library of 222 single alanine substitution mutants (all codons save for the start, stop and naturally occurring alanine) was generated and sequenced. To facilitate the identification of transformants carrying the mutated codon, a recipient strain was created with both the inducible *dnaD-ssrA* complementation system and the *dnaD* operon replaced by *bgaB* (encoding the enzyme β-galactosidase) (Supplementary Figure S3). Thus, replacement of *bgaB* with *dnaD* mutants can be detected on selective media supplemented with a chromogenic substrate (e.g. white colonies, Figure 1B) and confirmed by chloramphenicol sensitivity.

Following construction of the *dnaD* alanine substitution library, cultures grown in a microtiter plate were monitored in a plate reader to assess the functionality of each mutant. The data revealed growth defects for several alanine substitutions, spread throughout the protein (Figure 1C–F). Immunoblotting was used to determine the expression of fourteen DnaD variants conferring a strong growth phenotype. The expression of five mutants within this set could not be detected (Supplementary Figure S4), therefore we focussed on alanine substitutions that were present at near the wild-type level (Figures 3B, 4C and I). After its completion, this systematic genetic analysis identified nine residues in DnaD that are essential for cell viability (Figure 1D–F and Supplementary Figure S4, Table S6).

DnaD essential mutants abolish DNA replication initiation

While essential for DNA replication initiation in *B. subtilis*, DnaD has also been implicated in other key cellular processes including replication restart, chromosome organization, and DNA repair (45,71–74). To ascertain whether *dnaD* alanine mutants were specifically impaired in DNA replication initiation, we characterized chromosome content in these strains using fluorescence microscopy.

During steady-state growth in defined minimal media, wild-type *B. subtilis* cells typically display a pair of chromosome origins per nucleoid (*ori:nuc*), each orientated towards one cell pole (75). In contrast, when chromosome replication is inhibited, nucleoids typically contain a single *oriC* signal located near the centre of the bulk DNA (Figure 2A) (76). Therefore, to evaluate the impact of *dnaD* mutants on DNA replication, a strain was constructed with a fluorescently labelled nucleoid associated protein (Hbs-GFP) to detect the chromosome (77) and a fluorescent reporter-operator system (*tetO* array with TetR-mCherry) (78) to detect the relative number of *oriC* regions in every cell (Figure 2B). Cells were imaged following repression of the ectopic *dnaD-ssrA* for 90 min. All *dnaD* alanine mutants produced a phenotype characteristic of non-replicating chromosomes, with well separated nucleoids often containing a single central TetR-mCherry focus (Figure 2C). Quantitative analysis of microscopy images showed that all mutants appeared to display fewer origins and a decrease in the number of nucleoids per cell (Figure 2D), resulting in a reduction of the *ori:nuc* ratio compared to wild-type DnaD (Figure 2E). These results are consistent with the model that the identified essential DnaD amino acids are required to initiate DNA replication *in vivo*.

A DnaD tetramer is necessary for DNA replication initiation *in vivo*

The crystal structure of $DnaD^{NTD}$ has been solved as a symmetric homodimer, while biochemical experiments and structural modelling suggest assembly into a tetramer or higher-order oligomer (47,48). Critically, the active form of DnaD *in vivo* was not known. The alanine scan showed that replacement of either Phe6 or Leu22 led to strong growth defects (Figures 1D and 3A), and immunoblotting indicated that these DnaD variants are expressed *in vivo* (Figure 3B). Mapping the residues onto the $DnaD^{NTD}$ crystal structure revealed that Leu22 is buried within the proposed dimerization interface while Phe6 is exposed towards the predicted dimer:dimer interface (Figure 3C) (47). Note that Figure 3C also highlights the positions of alanine substitution variants that, while viable, were observed to alter colony morphology and to decrease the frequency of DNA replication initiation (Supplementary Figure S5). The location of these residues suggests they may play a role in DnaD homo-oligomerization.

To begin assessing the DnaD self-interaction, a bacterial two-hybrid assay was employed. Full-length *dnaD* alleles were fused to catalytically complementary fragments of the *Bordetella pertussis* adenylate cyclase (T25 and T18) (79). Two-hybrid analysis showed that wild-type DnaD and $DnaD^{F6A}$ self-interact, whereas $DnaD^{L22A}$ has lost this capability (Figure 3D). Both $DnaD^{F6A}$ and $DnaD^{L22A}$ were able to interact with wild-type DnaD, indicating that they were being stably expressed in the heterologous host (Figure 3D). The lack of self-interaction observed for the $DnaD^{L22A}$ variant suggests that Leu22 is a key residue involved in DnaD dimerization, consistent with previous structural data (47).

To further interrogate the quaternary structure of DnaD, we purified $DnaD^{L22A}$ and $DnaD^{F6A}$ and characterised these variants by size exclusion chromatography (SEC) (80) followed by multiple angle light scattering (MALS) (81). Wild-type DnaD was observed to run as a tetramer of approximately 113 kDa (theoretical molecular weight of 110 kDa) (Figure 3E and Supplementary Figure S6A). SEC-MALS analysis showed that >50% of $DnaD^{L22A}$ was present as a 29 kDa monomer, whereas $DnaD^{F6A}$ was eluted exclusively as 57 kDa species, consistent with the protein forming a homodimer (Figure 3E and Supplementary Figure S6A). It is unsurprising that $DnaD^{L22A}$ retains some ability to assemble into a tetramer (Figure 3E), as the substitution of leucine for alanine would not be expected to sterically disrupt the extensive dimer interface (Figure 3C) (47). Consistent with SEC-MALS, the dimerization capability of $DnaD^{L22A}$ was found to be poor using the amine-specific crosslinker bis(sulfosuccinimidyl)suberate (BS_3), while $DnaD^{F6A}$ was competent to form a dimer (Fig-

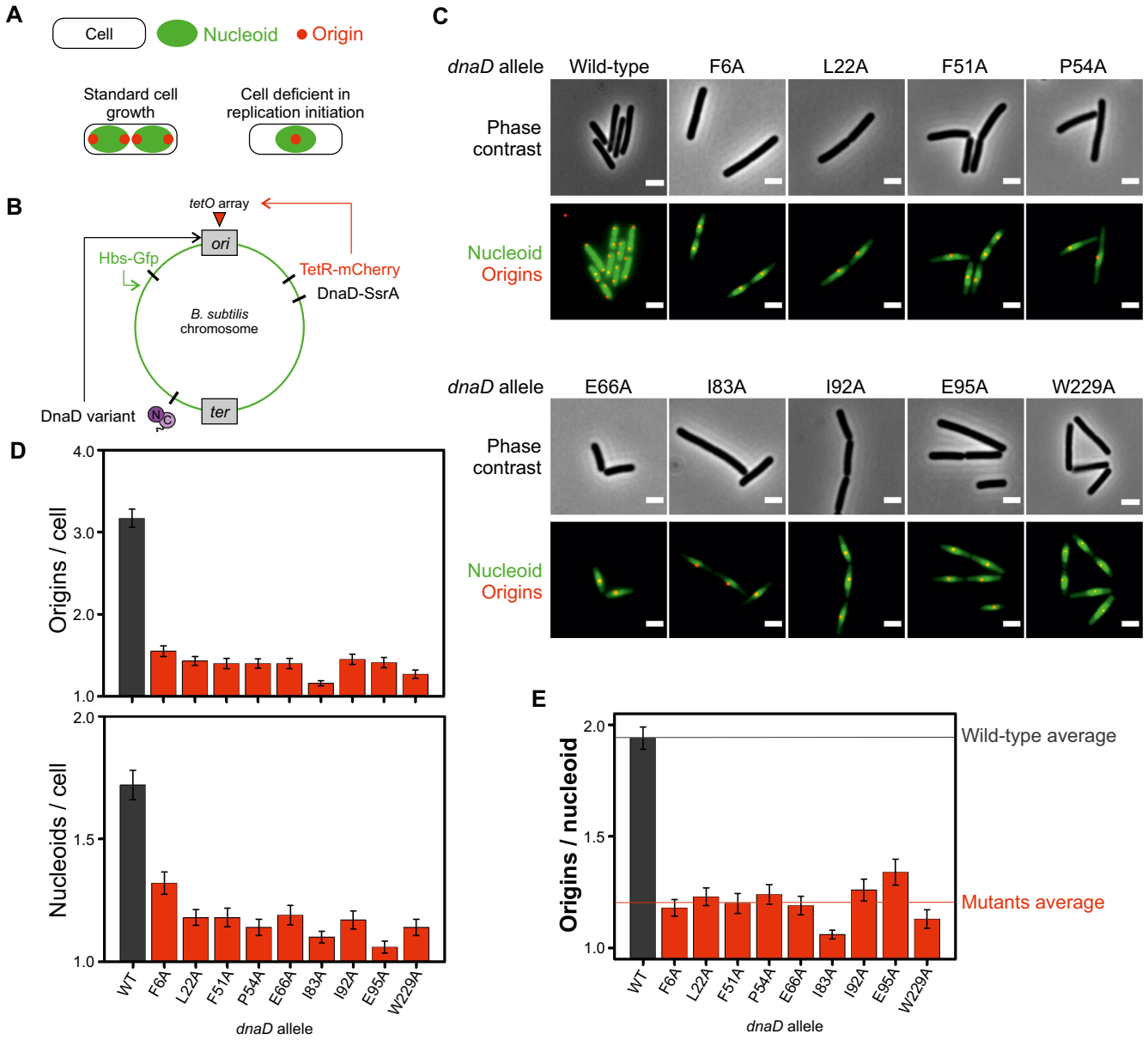

Figure 2. Lethal alanine substitutions in DnaD are defective in DNA replication initiation. (**A**) Schematics of the number of origins and nucleoids showing the typical patterns associated with cells displaying a normal growth phenotype or cells that are deficient in replication initiation. (**B**) Schematics of the dual fluorescence system engineered to label chromosome origins and the nucleoid. TetR-mCherry (red fluorescence) is constitutively expressed and binds an array of *tetO* sites located near the origin of replication. Hbs-GFP (green fluorescence) is constitutively expressed, non-specifically binds double-stranded DNA, and allows visualisation of the nucleoid. (**C**) Representative images of *dnaD* essential substitutions observed by fluorescence microscopy via the system described in (A). Red dots show chromosome origins and the green signal the nucleoid. Wild-type corresponds to a strain encoding the ectopic *dnaD-ssrA* cassette that was removed from IPTG and relied on the endogenous copy of wild-type *dnaD* (CW517). F6A (CW540), L22A (CW536), F51A (CW534), P54A (CW539), E66A (CW538), I83A (CW533), I92A (CW537), E95A (CW532), W229A (CW535). (**D**) Number of origins per cell (top) and nucleoids per cell (bottom) corresponding to the single-cell image analysis on DnaD variants from the experiments shown in (C). (**E**) Origin per nucleoid ratios corresponding to the single-cell image analysis performed on the data obtained from experiments shown in (C). Error bars in (D, E) show the standard error of the mean for at least two biological replicates where over 100 cells were counted for *dnaD* wild-type and mutant backgrounds.

ure 3F). Returning to the *dnaD* alanine scan, we appreciated that $dnaD^{K3A}$ was also lethal, albeit poorly expressed *in vivo* (Supplementary Figure S4). Nonetheless, recombinant $DnaD^{K3A}$ could be purified and like $DnaA^{F6A}$, BS_3 crosslinking showed that $DnaD^{K3A}$ was competent to form a dimer but not a tetramer (Figure 3F).

Taken all together, the data indicate that DnaD oligomerization is mediated by the N-terminal domain, with Leu22 required for dimerization and Lys3/Phe6 required for tetramerization (Figure 3G). Moreover, the results suggest that adopting a tetrameric quaternary state is necessary to support DNA replication initiation *in vivo*.

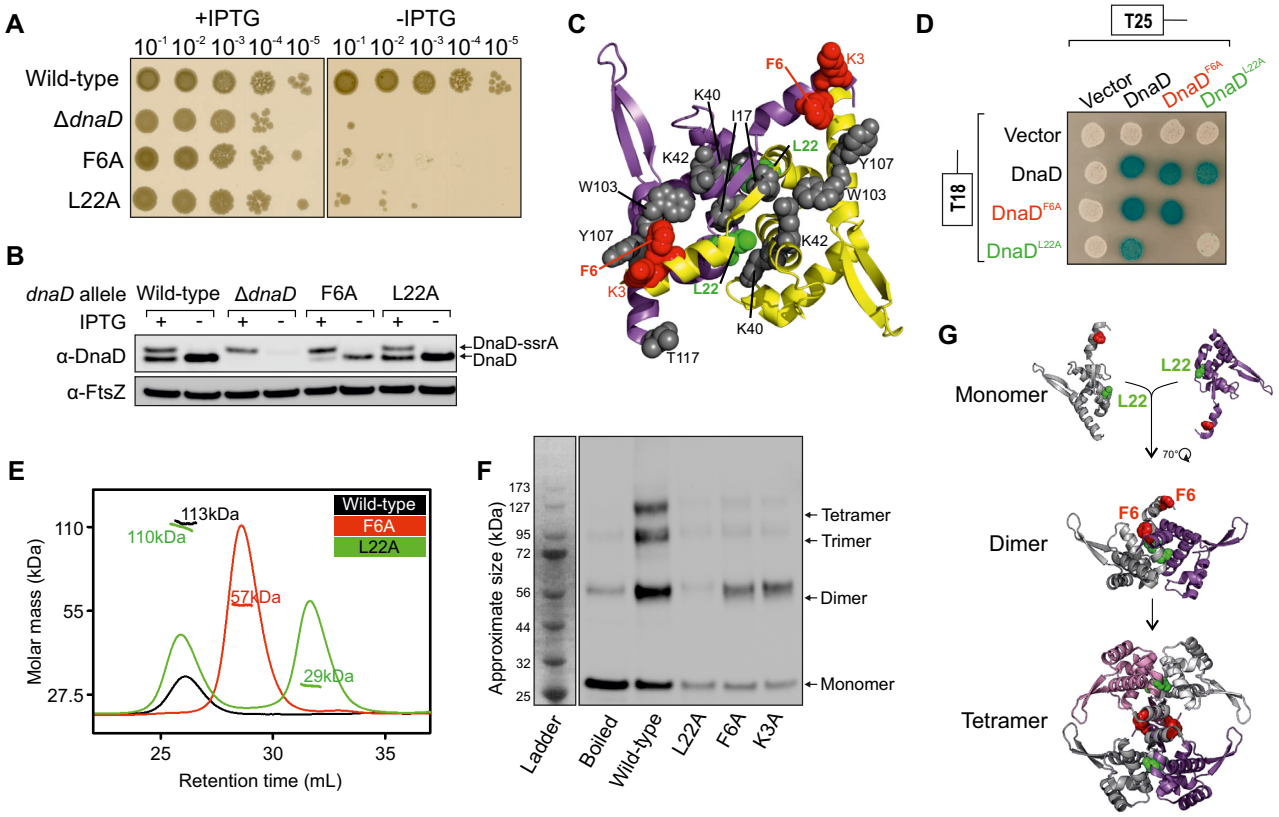

Figure 3. Lethal alanine substitutions in DnaD disrupt tetramer formation. (**A**) Spot titre analysis showing that substitutions *dnaD*^{F6A} (CW310) and *dnaD*^{L22A} (CW292) produced a lethal phenotype *in vivo*. The presence or absence of IPTG indicates the induction state of the ectopic *dnaD-ssrA* cassette. Wild-type (CW162), *ΔdnaD* (CW197). (**B**) Immunoblot showing that DnaD^{F6A} and DnaD^{L22A} are expressed *in vivo* and remain stable upon depletion of the ectopic DnaD-ssrA copy (no IPTG condition). Detection of the tubulin homolog FtsZ was used as a loading control. Strains are the same as used in (A). (**C**) DnaD N-terminal domain crystal structure (PDB 2v79) showing an extensive interface mapped with residues that produced a different phenotype than wild-type after the alanine scan. Purple and yellow subunits indicate individual protomers. Residues are marked as red for lethal and grey for altered growth (translucent/heterogeneous phenotype or slow growth). (**D**) Bacterial two-hybrid assay showing the effect of mutants DnaD^{L22A} and DnaD^{F6A} on self-interaction. White spots indicate a lack of interaction and coloured spots the interaction between two protein variants. White colonies observed with empty vectors indicate that the detected interactions are specific. Plasmids used in this assay are listed in Supplementary Table S2. (**E**) SEC-MALS analysis of purified DnaD protein variants. The UV spectrum (continuous lines) was normalised as a relative refraction index and the molar mass corresponding to each protein is shown as shorter/thicker lines overlapping the different peaks. Masses corresponding to each peak are annotated on the plot. (**F**) Immunoblot following migration and transfer of BS_3 crosslinked DnaD species using SDS-PAGE. The ladder indicates the approximate size of fragments. The 'Boiled' lane corresponds to a wild-type DnaD sample that was boiled prior to crosslinking. SDS-PAGE confirmed that equal amounts of proteins were loaded (Supplementary Figure S6B). (**G**) Schematics of DnaD N-terminal domain oligomerization pathway involving key residues F6 and L22. DnaD^{L22} allows formation of a dimer and DnaD^{F6} contributes to further assembly into a tetramer.

The interaction between DnaD^{CTT} and DnaB is necessary for DNA replication initiation *in vivo*

The alanine scan indicated that a cluster of residues in the unstructured C-terminal tail of DnaD are critical for cell growth, particularly Trp229 which is essential and well expressed (Figure 4A-C). Phylogenetic analysis indicates that Trp229 is conserved in species harbouring both *dnaD* and *dnaB*, but not *dnaD* alone (Figure 4D and Supplementary Table S7), suggesting that the DnaD^{CTT} could be an interaction site for DnaB.

To test this hypothesis, two-hybrid analysis was used to probe for protein:protein interactions. However, it was previously reported that interactions between full-length *B. subtilis* DNA replication initiation proteins could not be detected (37), consistent with the observation that expression of *B. subtilis* initiator proteins in *E. coli* is toxic (82,83). We hypothesised that this phenotype arises from *B. subtilis* proteins interfering with DNA replication initiation in *E. coli* (e.g. *B. subtilis* DnaA binds to *E. coli* DnaA-boxes but cannot unwind *E. coli oriC*) (83). To circumvent these challenges and allow bacterial two-hybrid analysis of full-length *B. subtilis* DNA replication initiation proteins, we constructed a derivative of the *E. coli* two-hybrid strain with a deletion of the *rnhA* gene (encoding for RNase HI). RNase HI degrades stable DNA-RNA hybrid structures such as R-loops (84). The knockout of *rnhA* in *E. coli* allows formation of R-loops, which can be used to initiate DNA replication independently of DnaA and *oriC* (85).

Using this system, an interaction between wild-type DnaD and DnaB proteins was detected (Figure 4E). Altering Trp229 to alanine or deleting the last eight amino acids of DnaD reduced and disrupted the interaction with DnaB, respectively (Figure 4E). It was also observed that the monomeric DnaD^{L22A} variant was unable to interact with DnaB, whereas the dimeric DnaD^{F6A} retained this ca-

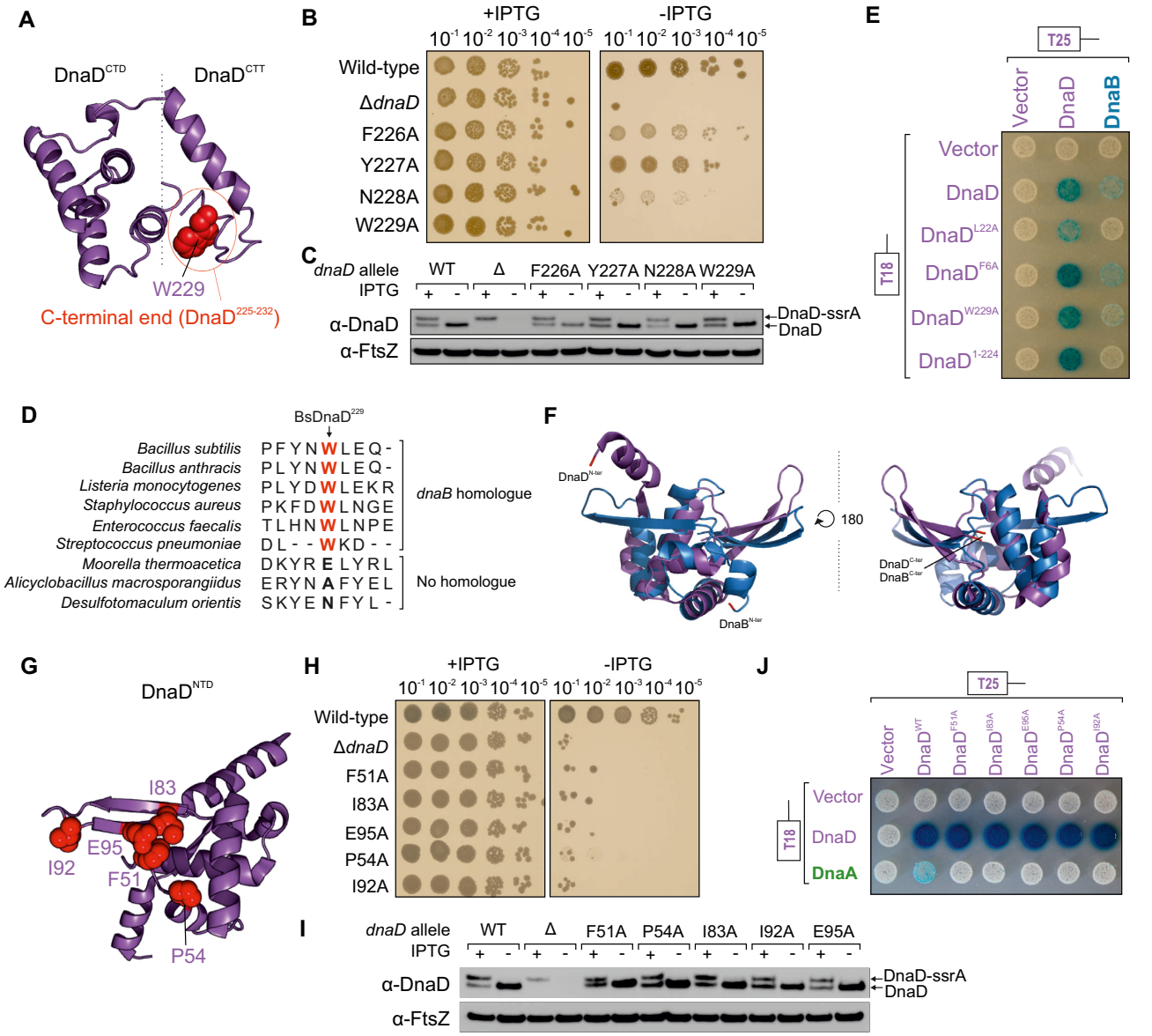

Figure 4. Lethal alanine substitutions in DnaD disrupt its interactions with DnaB and DnaA. (**A**) Essential residues of DnaD, required for the interaction with DnaB, mapped onto a DnaD$^{CTD/CTT}$ model. (**B**) Spot titre analysis showing that substitutions in DnaD^{CTT} variably affect cell growth *in vivo*. The presence or absence of IPTG indicates the induction state of the ectopic *dnaD-ssrA* cassette. Wild-type (CW162), *ΔdnaD* (CW197), F226A (CW284), Y227A (CW317), N228A (CW285), W229A (CW286). (**C**) Immunoblot showing that DnaD variants shown in (B) are expressed *in vivo* and remain stable upon depletion of the ectopic DnaD-ssrA copy (no IPTG condition). Detection of the tubulin homolog FtsZ was used as a loading control. Strains are the same as used in (B). (**D**) Protein sequence alignment of DnaD homologs showing that *B. subtilis* DnaD^{W229} is particularly conserved in species that also harbour a copy of DnaB. (**E**) Bacterial two-hybrid assay showing loss of interaction between DnaD variants and DnaB in the context of full-length proteins. White spots indicate a lack of interaction and coloured spots the interaction between two protein variants. White colonies observed with empty vectors indicate that the detected interactions are specific. Plasmids used in this assay are listed in Supplementary Table S2. (**F**) Structural alignment showing that the N-terminal domains of DnaD (PDB 2v79) and DnaB (PDB 5wtn) significantly overlap. (**G**) Essential residues of DnaD, required for the interaction with DnaA, mapped onto the DnaD^{NTD} crystal structure (PDB 2v79). (**H**) Spot titre analysis showing that substitutions in DnaD^{NTD} shown in (G) produced a lethal phenotype *in vivo*. The presence or absence of IPTG indicates the induction state of the ectopic *dnaD-ssrA* cassette. Wild-type (CW162), *ΔdnaD* (CW197), F51A (CW174), P54A (CW295), I83A (CW170), I92A (CW297), E95A (CW166). (**I**) Immunoblot showing that DnaD variants shown in (H) are expressed *in vivo* and remain stable upon depletion of the ectopic DnaD-ssrA copy (no IPTG condition). Detection of the tubulin homolog FtsZ was used as a loading control. Strains are the same as used in (H). (**J**) Bacterial two-hybrid assay showing loss of interaction between DnaD^{NTD} variants and DnaA in the context of full-length proteins. White spots indicate a lack of interaction and coloured spots the interaction between two protein variants. White colonies observed with empty vectors indicate that the detected interactions are specific. Plasmids used in this assay are listed in Supplementary Table S2.

pability, indicating that DnaB recognition requires DnaD assembly into a homodimer (Figure 4E). All DnaD variants retained a self-interaction with the wild-type protein, showing that they were being expressed (Figure 4E). These results suggest that the interface between the distal end of $DnaD^{CTT}$ and DnaB is essential for DNA replication initiation *in vivo*.

Previous studies using protein truncation variants indicated that the $DnaD^{NTD}$ interacts with $DnaB^{NTD}$ (37). The observation that mutations in the $DnaD^{CTT}$ abolish the interaction with DnaB, while leaving the $DnaD^{NTD}$ intact, suggests that different DnaD:DnaB complexes are being detected in these assays. We also note that the N-terminal domains of DnaD and DnaB share structural homology (Figure 4F) and that both promote dimerization/tetramerization (42,43), such that the truncated variants used in previous studies (37) may be able to interact differentially in a two-hybrid assay.

The interaction between $DnaD^{NTD}$ and DnaA is necessary for DNA replication initiation *in vivo*

Models for the interaction between DnaD and DnaA have been proposed based on binding experiments using truncated proteins. These studies indicated that residues in the $DnaD^{NTD}$ (37) and the $DnaD^{CTD}$ (40) each contributed to DnaA binding. From the alanine scan it was observed that three of the residues at the proposed DnaA interface of the $DnaD^{NTD}$ are essential (Phe51, Ile83, Glu95). Additionally, we identified two other lethal and stably expressed substitutions ($DnaD^{P54A}$ and $DnaD^{I92A}$) that mapped near these sites on the structure (Figure 4G-I), suggesting they could also be involved in forming the DnaA interface.

In contrast, none of the residues in the proposed DnaA binding region of the $DnaD^{CTD}$ were found to be essential (Supplementary Figure S7A–C). To investigate whether the interface between $DnaD^{CTD}$ and DnaA was robust and single alanine substitutions were insufficient to disrupt binding, DnaD variants encoding multiple alanine substitutions were constructed (*dnaD*$^{L129A/I132A}$, *dnaD*$^{Y130A/E134A/E135A}$, *dnaD*$^{I132A/E134A/E135A}$, *dnaD*$^{K164A/K168A/E169A/V171A}$) (Supplementary Figure S7D–G). However, all of these *dnaD* alleles were viable and supported normal growth (Supplementary Figure S7C). These results indicate that the previously identified interface between DnaA and the $DnaD^{CTD}$ (40) is not essential for DNA replication initiation *in vivo*. The $DnaD^{CTD}$–DnaA interaction could play an auxiliary role that assists DnaD binding DnaA, or it could become important during certain environmental conditions or cell stresses.

Two-hybrid analysis was used to investigate whether lethal alanine substitutions in $DnaD^{NTD}$ perturb the interaction with DnaA. While an interaction between the full-length wild-type DnaD and DnaA proteins was detected, alanine substitutions within the proposed $DnaD^{NTD}$ interface for DnaA abrogated the two-hybrid signal (Figure 4J). All $DnaD^{NTD}$ variants retained the ability to self-interact, indicating that they were being stably expressed in *E. coli* (Figure 4J), and size exclusion chromatography confirmed that the purified DnaD variants were tetrameric (Supplementary Figure S6C). These results confirm and extend previous reports identifying the interface between DnaA and $DnaD^{NTD}$ (37), and they show for the first time that this interaction is essential for DNA replication initiation *in vivo*.

The interaction between $DnaA^{DI}$ and DnaD is necessary for DNA replication initiation *in vivo*

Having identified the essential surface of DnaD required to interact with DnaA, we next determined essential residues in DnaA required to interact with DnaD. Previous two-hybrid and NMR studies implicated residues on the surface of $DnaA^{DI}$ that interact with DnaD (37,40). To investigate the physiological relevance of the proposed $DnaA^{DI}$ interface, we replaced the endogenous *dnaA* gene with mutants encoding alanine substitutions at key residues (*dnaA*^{T26A}, *dnaA*^{W27A}, *dnaA*^{F49A}) (Figure 5A).

To enable identification of essential amino acid residues without selecting for suppressor mutations, we utilized a strain in which DNA replication can initiate from a plasmid origin (*oriN*) integrated into the chromosome (Figure 5B) (24). The activity of *oriN* requires its cognate initiator protein RepN, and both factors act independently of *oriC*/DnaA (note the RepN/*oriN* system also requires DnaD and DnaB for function) (Supplementary Figure S8) (86). Expression of *repN* was placed under the control of an IPTG-inducible promoter, thus permitting both the introduction of mutations into *dnaA* and their subsequent analysis following removal of the inducer to repress *oriN* activity. Cultures were grown overnight in the presence of IPTG and then serially diluted onto solid media with and without the inducer. The results show that the *dnaA*^{T26A}, *dnaA*^{W27A} and *dnaA*^{F49A} mutants all inhibited colony formation over a range of temperature (Figure 5C and Supplementary Figure S9A-B). Immunoblot analysis confirmed that all of the DnaA variants were expressed at a level similar to wild-type (Figure 5D). This indicates that residues Thr26, Trp27 and Phe49 are essential for DnaA activity *in vivo.*

Two-hybrid analysis confirmed that alanine substitutions in DnaA at either Thr26, Trp27 or Phe49 inhibit the interaction with DnaD (Figure 5E). These $DnaA^{DI}$ variants retained the ability to interact with wild-type DnaA protein and with DnaB, indicating that they were stably expressed (Figure 5E). The data suggest that the essential residues Thr26, Trp27, Phe49 of DnaA are required for the interaction with DnaD (Figure 5E).

To investigate whether $DnaA^{DI}$ and $DnaD^{NTD}$ were sufficient to form a complex, pull-down assays between protein domains His_6-$DnaA^{DI}$ and $DnaD^{NTD}$ were performed (Supplementary Figure S9C). Following co-expression of His_6-$DnaA^{DI}$ and $DnaD^{NTD}$ in *E. coli*, cells were lysed and His_6-$DnaA^{DI}$ was captured using an immobilized nickel affinity chromatography spin column. While the wild-type $DnaD^{NTD}$ was able to bind wild-type His_6-$DnaA^{DI}$, alanine substitutions in either protein greatly reduced the retention of $DnaD^{NTD}$ (Figure 5F). Analysis of cell lysates by SDS-PAGE revealed that all protein domains were being overexpressed to similar levels (Supplementary Figure S9D) and immunoblotting confirmed the identity of each polypeptide (Supplementary Figure S9E). These studies support and extend the previously proposed model for $DnaA^{DI}$ interacting with $DnaD^{NTD}$ (37), and they show for the first time that

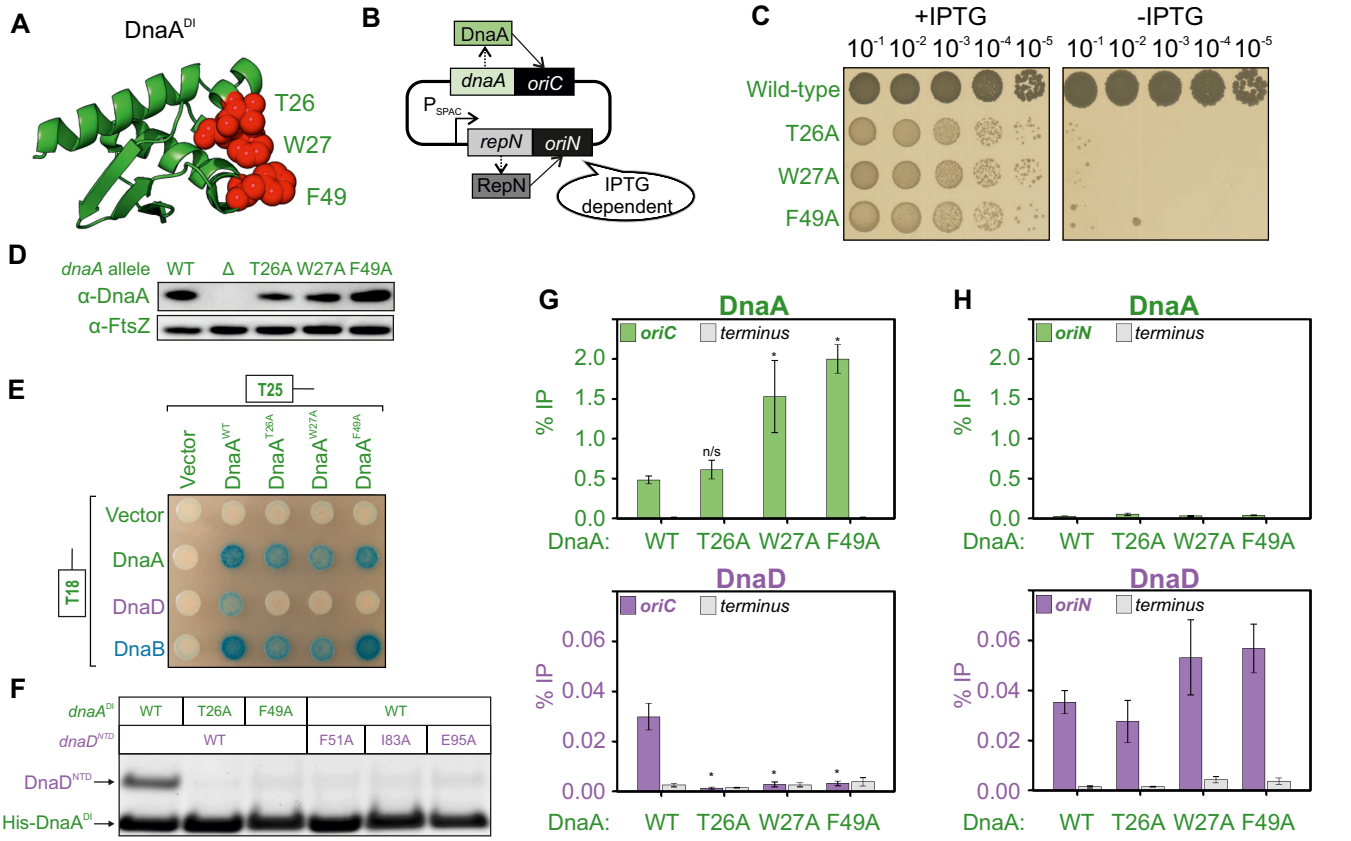

Figure 5. The interaction between DnaA domain I and DnaD^{NTD} is essential for DnaD recruitment to *oriC*. (**A**) Essential residues of DnaA, required for the interaction with DnaD, mapped onto the DnaA^{DI} crystal structure (PDB 4tps). (**B**) Schematics of the inducible *repN*/*oriN* system used to bypass mutations affecting DnaA activity in *B. subtilis*. Replication via *oriN* is turned on and off in the presence and absence of IPTG, respectively. (**C**) Spot titre analysis showing that DnaA^{DI} variants produced a lethal phenotype *in vivo*. The presence or absence of IPTG indicates the induction state of the *repN*/*oriN* system. Wild-type (HM1108), T26A (HM1540), W27A (HM1541), F49A (HM1542). (**D**) Immunobloting shows that DnaA^{DI} variants were expressed at a similar level to wild-type in the context of the *oriN* strain. Detection of the tubulin homolog FtsZ was used as a loading control. Wild-type (HM1524), Δ*dnaA* (HM1424), T26A (HM1537), W27A (HM1538), F49A (HM1539). (**E**) Bacterial two-hybrid assay showing the loss of interaction between DnaA variants and DnaD in the context of full-length proteins. The interaction between DnaA and DnaB was unaffected by DnaA^{DI} variants. White spots indicate a lack of interaction and blue spots the interaction between two protein variants. White colonies observed with empty vectors indicate that the detected interactions are specific. (**F**) Pull-down assay (stained SDS-PAGE) showing loss of interaction between His$_6$-DnaA^{DI} and DnaD^{NTD} when using variants of DnaA or DnaD. Plasmids used in (E-F) are listed in Supplementary Table S2. (**G**) ChIP analysis showing that DnaA protein variants remain enriched at *oriC*, whereas DnaD is not recruited to *oriC* when using DnaA^{DI} mutants. Primers used for the origin anneal within the *incC* region. * shows a *P*-value < 0.02 and n/s a non-significant difference. Wild-type (HM949), T26A (HM1537), W27A (HM1538) and F49A (HM1539). (**H**) Control for the ChIP analysis shown in (G). DnaA protein variants (wild-type, T26A, W27A and F49A) are not recruited to *oriN* while DnaD remains enriched at this site. Samples are the same as used in (G) with primers annealing within *oriN*.

this interaction is essential for DNA replication initiation *in vivo*.

The interaction of DnaA^{DI} with DnaD^{NTD} is required to recruit DnaD to the chromosome origin

DnaA binding to *oriC* is required to detect the enrichment of DnaD at the replication origin (38), therefore we wondered whether the DnaA^{DI}–DnaD^{NTD} interaction described above was essential for DnaD recruitment. To test this hypothesis, we employed chromatin immunoprecipitation followed by quantitative PCR (ChIP-qPCR). Here, to support growth of lethal *dnaA* mutants, a strain harbouring a constitutively active version of *oriN* within the chromosome was used (87). In all cases, DnaA^{DI} variants remained specifically enriched at *oriC* while recruitment of DnaD was abolished (Figure 5G). The accumulation of DnaA^{W27A} and DnaA^{F49A} at *oriC* was reminiscent of previous ChIP experiments showing that DnaA becomes enriched at the origin when DNA replication initiation is blocked (38,45,88). Note that in these strains DnaD remained enriched at *oriN,* as expected (Figure 5H) (45).

The ChIP data are consistent with the model that an essential function of the DnaA^{DI}–DnaD^{NTD} interaction is to recruit DnaD to *oriC*. However, an essential activity of DnaA is also to unwind *oriC*, and it has been suggested that DnaA^{DI} has an affinity for ssDNA (34). It was conceivable that a defect in *oriC* unwinding might indirectly impact DnaD recruitment. To determine whether residues in DnaA^{DI} are required for *oriC* opening, a DNA strand separation assay was employed (26). Here recombinant DnaA proteins are incubated with fluorescently labelled oligonucleotide scaffolds that mimic *oriC*, and DNA strand separation is detected using a platereader (Supple-

mentary Figure S10A). As was reported using a truncated DnaA protein from *Aquifex aeolicus* (22), *B. subtilis* DnaA domains I and II are not necessary for strand separation activity (Supplementary Figure S10, $DnaA^{III–IV}$). This result supports the proposal that the essential function of these $DnaA^{DI}$-residues is DnaD recruitment. Intriguingly, the surface of $DnaA^{DI}$ interacting with DnaD is also the binding site for the developmentally expressed DNA replication inhibitor SirA, raising the possibility that SirA could directly compete with DnaD for binding DnaA (Figure 6A) (32,33).

SirA binding to DnaA inhibits recruitment of DnaD and DnaB to *oriC*

During endospore development *B. subtilis* requires two chromosomes, one for each differentiated cell type (89). To help ensure diploidy after executing the commitment to sporulate, cells express the negative regulator of DNA replication initiation SirA (51,90). It was proposed that SirA represses DNA replication initiation by inhibiting DnaA binding to *oriC* (33). However, SirA binds to $DnaA^{DI}$ (32), distal to the established DNA binding motifs of DnaA. Thus, the mechanism for how SirA inhibits DnaA recruitment at *oriC* was unclear. Considering the data presented above, we explored the alternative hypothesis that SirA binding to $DnaA^{DI}$ occludes DnaD, thereby repressing DNA replication initiation by specifically inhibiting recruitment of DnaD to *oriC*.

Using a strain containing an ectopic copy of *sirA* under the control of an IPTG-inducible promoter, SirA was expressed for 30 min during mid-exponential growth. Previous studies showed that DnaA-dependent replication initiation was blocked under these conditions (51,90). ChIP of wild-type DnaA revealed stable enrichment at *oriC* following SirA expression (Figure 6B), indicating that under these conditions SirA does not inhibit DnaA binding to DNA. ChIP of DnaD showed enrichment was abolished, consistent with the model that SirA inhibits DnaD binding to DnaA. Furthermore, enrichment of the helicase loader DnaB at *oriC*, which requires prior binding of DnaD (38), was also lost following induction of *sirA* (Supplementary Figure S11). ChIP experiments were then performed using strains harbouring the variants $DnaA^{N47S}$ and $DnaA^{A50V}$, which are resistant to SirA inhibition (33). Enrichment of DnaD at *oriC* was restored by $DnaA^{N47S}$ and $DnaA^{A50V}$, to a degree that correlated with the penetrance of the *dnaA* allele (Figure 6B) (32). Therefore, expression of SirA during exponential growth appears to specifically block DnaD recruitment to *oriC*.

Rapid loss of DnaD enrichment at *oriC* during sporulation depends on SirA

To investigate the impact of SirA during sporulation, we probed the recruitment of DnaA and DnaD to *oriC* in cells induced to sporulate synchronously by the resuspension method (Supplementary Figure S12) (60,61). Because cells undergo a nutrient downshift upon resuspension in sporulation medium, they were allowed to equilibrate for one hour before samples were taken. ChIP analysis showed that in a wild-type strain, both DnaA and DnaD are depleted from *oriC* through the course of sporulation (Figure 6C, D and Supplementary Figure S13A, B). In a Δ*sirA* mutant both proteins remained relatively enriched at *oriC* during the first two hours of the developmental process, followed by their eventual depletion (Figure 6C, D). The apparent timing of SirA activity is consistent with previous reports indicating that *sirA* is induced early during sporulation (51,91). Strikingly, during the first two hours of sporulation in a strain expressing the $DnaA^{N47S}$ variant that is resistant to SirA, the relative enrichment of DnaD at *oriC* increased while for wild type it decreased (Figure 6E, F; Supplementary Figure S13C, D). ChIP analysis at later timepoints showed that recruitment of DnaD to the origin was eventually reduced (Figure 6F), suggesting that additional factors mediate longer-term depletion of initiation proteins from the replication origin. To assess the impact of SirA on DNA replication during the early stages of sporulation, we imaged wild-type and Δ*sirA* cells harbouring a *gfp-dnaN* fusion, enabling us to visualise the sliding clamp processivity factor associated with replisomes (92). Consistent with previous studies (51), in the Δ*sirA* mutant there was a greater number of cells with GFP-DnaN foci compared to the wild-type strain (Figure 6G, H). Together, the results indicate that SirA is required for the rapid depletion of DnaD from the replication origin and arrest of DNA replication during the early stages of sporulation.

SirA and DnaD compete for binding to $DnaA^{DI}$

To investigate whether SirA and DnaD binding to $DnaA^{DI}$ is mutually exclusive, we performed a competition experiment. A strain was engineered with ectopic copies of *sirA* and *dnaD* under the control of distinct inducible promoters (IPTG and xylose, respectively). While expression of SirA alone inhibited growth, co-expression with DnaD significantly ameliorated this effect (Figure 7A and Supplementary Figure S14A–C). In contrast, expression of DnaD variants defective for binding DnaA ($DnaD^{F51A}$, $DnaD^{I83A}$ or $DnaD^{E95A}$) could not alleviate the growth inhibition caused by SirA (Supplementary Figure S14D, E). Marker frequency analysis following 90 min induction of *sirA* and/or *dnaD* showed that SirA expression reduced DNA replication initiation, while co-expression with DnaD partially relieved this repression (Figure 7B). Taken together, our results suggest that SirA binds to $DnaA^{DI}$ and occludes the essential DnaA:DnaD interface (Figure 7C), thus providing a molecular mechanism for SirA mediated inhibition of DNA replication initiation.

DISCUSSION

The molecular basis underpinning how bacteria orchestrate and regulate the onset of DNA replication throughout growth and development was unclear. Here, characterization of the essential DNA replication initiation protein DnaD identified amino acids required for forming a homo-tetramer, as well as for interacting with the *B. subtilis* replication initiation proteins DnaA and DnaB (Figure 8A). These findings illuminate specific activities of DnaD required during DNA replication initiation in *B. subtilis*,

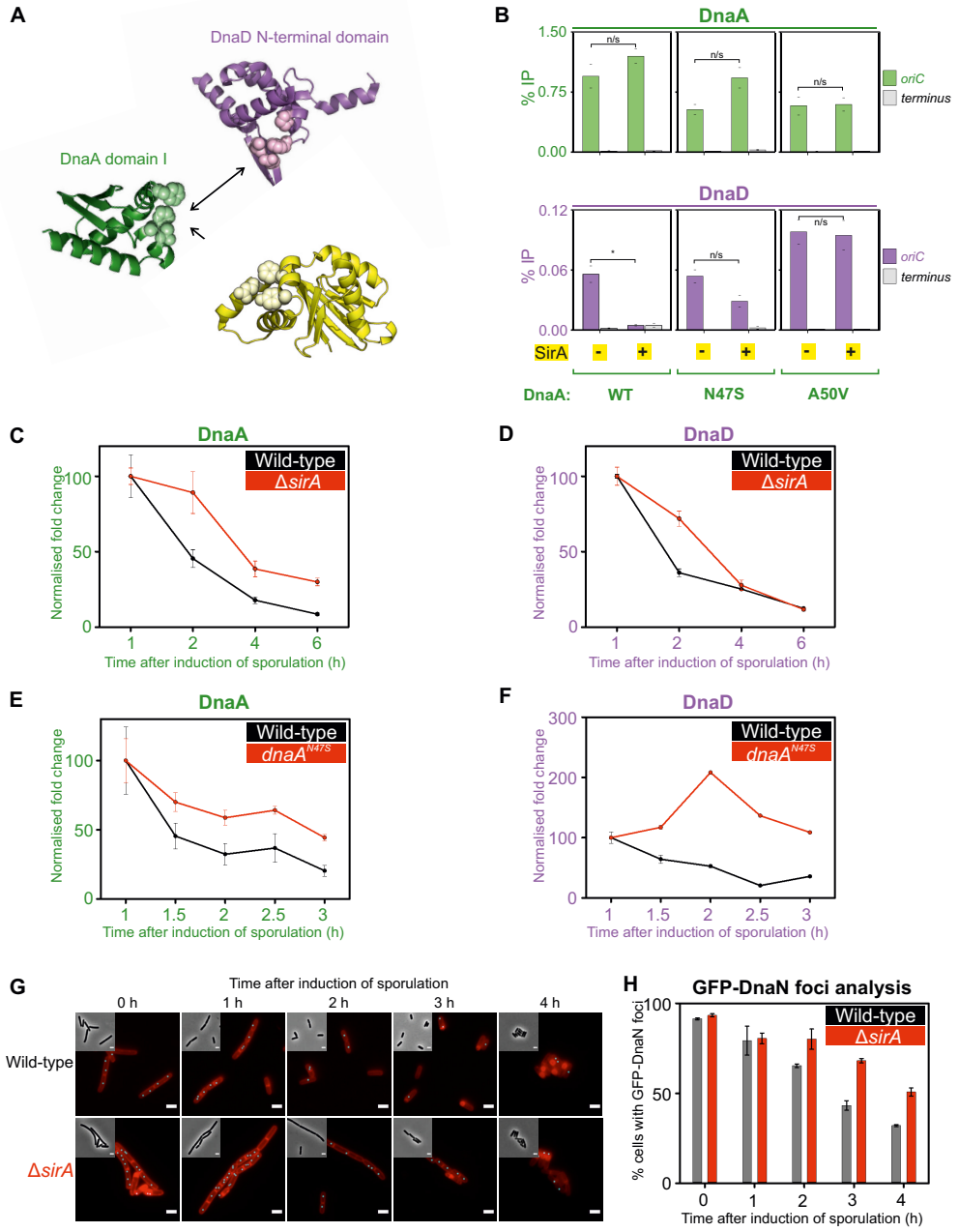

Figure 6. SirA binds to DnaA^{DI} and inhibits DnaD recruitment to *oriC* during sporulation. (**A**) Crystal structures of DnaD^{NTD} (PDB 2v79) and DnaA^{DI}-SirA (PDB 4tps) highlighting residues at the protein:protein interfaces responsible for the DnaA^{DI}-DnaD^{NTD} and DnaA^{DI}-SirA interactions. (**B**) ChIP analysis showing that DnaA protein variants remain enriched at *oriC* following overexpression of SirA, whereas DnaD is only recruited to the origin when *sirA* is not overexpressed or when using *dnaA* alleles suppressing the interaction between DnaA and SirA. * shows a *P*-value < 0.001 and n/s a non-significant difference. Wild-type (HM1565), suppressor alleles of the DnaA-SirA interaction: *dnaA*^{N47S} (SF27) and *dnaA*^{A50V} (SF24). (**C, D**) Depletion of DnaA (C) and DnaD (D) from the origin of replication *oriC* throughout the course of sporulation in wild-type (*B. subtilis* 168CA) or mutant cells lacking a copy of *sirA* (CW1065). Fold enrichment of DnaA/DnaD at the origin compared to levels of protein recruited to the terminus was calculated as an *ori*/Ter ratio and normalised to the 1h time point after the induction of sporulation by the resuspension method. Strains are the same as used in Supplementary Figure S12. (**E**) Depletion of DnaA from *oriC* during the early stages of sporulation in wild-type (*B. sub*tilis 168CA) or mutant cells where DnaA cannot interact with SirA (*dnaA*^{N47S} - CW1073). The normalised fold change indicates that DnaA remains relatively enriched at the origin by two hours after the induction of sporulation by the resuspension method. (**F**) Enrichment of DnaD at *oriC* during the early stages of sporulation in mutant cells where DnaA cannot interact with SirA (*dnaA*^{N47S} - CW1073) or depletion as expected in wild-type cells (*B. subtilis* 168CA). The normalised fold change indicates that DnaD is relatively enriched at the origin by two hours after the induction of sporulation by the resuspension method. Error bars shown in (C–F) represent propagated standard errors of the mean over three biological repeats. (**G**) Representative microscopy images showing GFP-DnaN foci (e.g. replisome marker) in wild-type or *ΔsirA* cells induced to sporulate by the resuspension method. Fluorescence microscopy images highlight the cell membrane and pre-spore in red and automatically detected GFP-DnaN foci as cyan dots. (**H**) Quantification of the presence of GFP-DnaN foci in single cells over time from the microscopy data shown in (G). Data analysis was performed from over 100 cells for each condition and error bars indicate the standard error of the mean over two biological repeats.

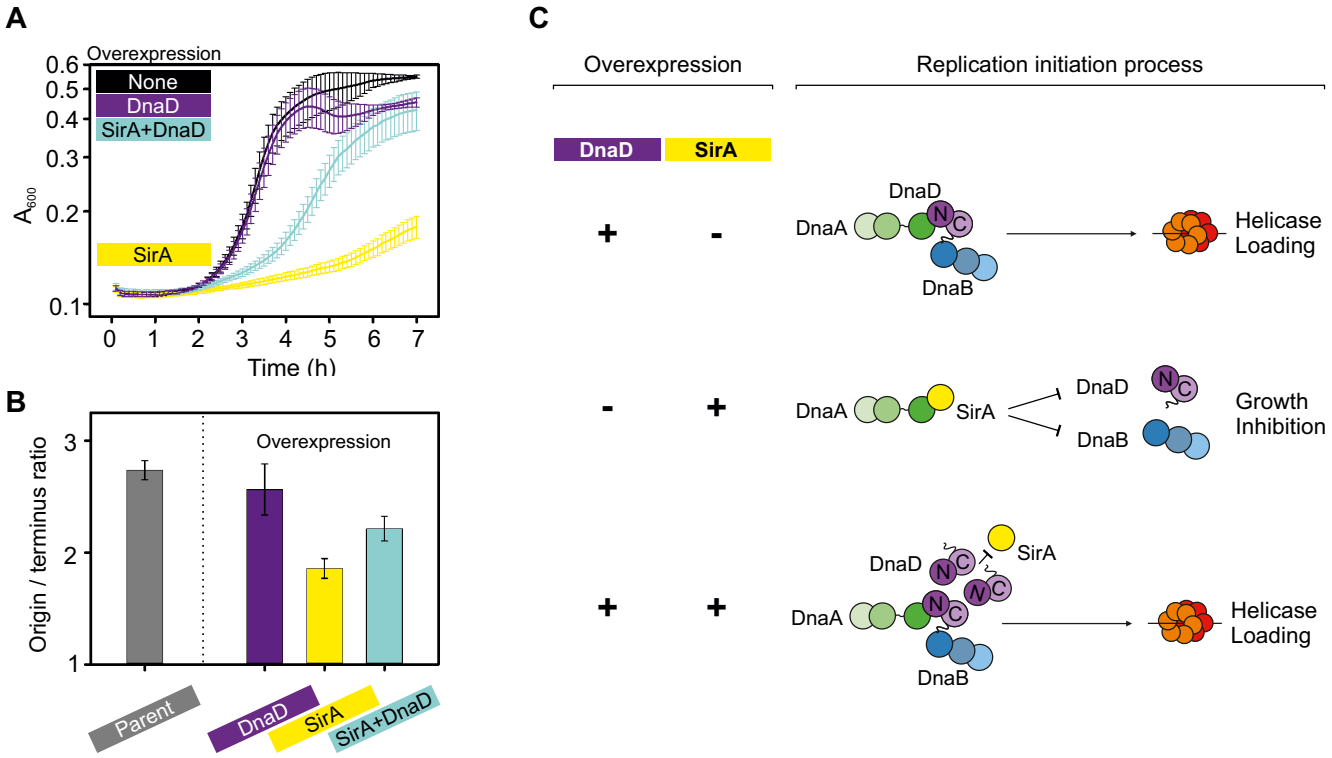

Figure 7. SirA and DnaD compete for binding to $DnaA^{DI}$. (**A**) Plate reader growth assay showing that overexpression of SirA inhibits growth, which can be partially rescued by simultaneous overexpression of DnaD (CW252). None indicates cells growing without inducer, DnaD overexpression was performed with 0.35% xylose, SirA overexpression with 0.035 mM IPTG, DnaD and SirA simultaneous overexpression with 0.35% xylose and 0.035 mM IPTG. Error bars indicate the standard error of the mean for at least three biological replicates. (**B**) Marker frequency analysis by quantitative PCR showing that overexpression of DnaD yields a similar *ori*:Ter ratio to the control strain (168CA), whereas overexpressing SirA strongly inhibits chromosome replication and simultaneous expression with DnaD partially restores it (CW252). (**C**) Schematic outcomes of the DnaD/SirA competition assay. The sole overexpression of DnaD does not affect bacterial growth and leads to helicase loading, whereas SirA overexpression inhibits growth via binding to $DnaA^{DI}$. This inhibition can be partially rescued and helicase loading restored when DnaD competes with SirA for $DnaA^{DI}$ binding.

which in turn engendered a model for the molecular mechanism used by SirA to regulate DNA synthesis during sporulation (Figure 8B).

The essential Leu22 was found to be specifically required for DnaD dimerization. This is in agreement with the location of Leu22 within the crystal structure of $DnaD^{NTD}$ (47). Leu22 is one of thirteen residues which are thought to become significantly buried upon dimer formation (47). We also note that while Ile17 was not essential, the $DnaD^{I17A}$ variant did produce a growth defect (Supplementary Figure S5) and this amino acid also becomes buried upon dimerization (47).

The essential Phe6 was found to be specifically required for DnaD tetramerization. Phe6 was previously postulated to play a role in dimer:dimer formation of $DnaD^{NTD}$ by interacting with residues in the winged-helix fold (47). Consistent with this, strains expressing alanine substitutions at Trp103 and Tyr107 (in the winged-helix) both produced growth defects (Supplementary Figure S5). Unexpectedly however, alanine substitutions at neither Thr14 nor Thr16 produced any phenotype in our screen; these had been suggested to pack onto a tight core of eight threonine side chains to stabilize the $DnaD^{NTD}$ tetramer (47). While a molecular understanding of DnaD tetramerization requires further structural work, the identification of specific DnaD variants blocked in oligomerization that are also defective for DNA replication initiation supports the model that the functional conformation of DnaD within the cell is a tetramer.

The C-terminal tail of DnaD was found to be required for orchestrating the DnaD:DnaB interaction, particularly the essential residue Trp229 (Figure 4A–E). Previously it was suggested that DnaB interacted with the $DnaD^{NTD}$, although a specific binding site was not delineated (37). Based on the observation that the $DnaD^{CTT}$ is essential and that it is required to interact with DnaB, we proposed that the $DnaD^{CTT}$ is the critical binding site for DnaB within the cell. Furthermore, the results of two-hybrid experiments suggest that DnaD dimer formation is required to bind DnaB, since the $DnaD^{L22A}$ monomer did not interact with DnaB while the $DnaD^{F6A}$ dimer did (Figure 4E). The next step in characterizing the DnaD:DnaB interaction will be to identify the complementary binding site for DnaD on DnaB.

An extensive $DnaD^{NTD}$ interface (Phe51, Pro54, Ile83, Ile92, Glu95; Figure 4G–I) is essential for viability and specifically required for interacting with DnaA, consistent with two-hybrid analysis (37). The complementary interface for DnaD on $DnaA^{DI}$ (Thr26, Trp27, Phe49) is also essential for viability, as well as for enrichment of DnaD at *oriC*

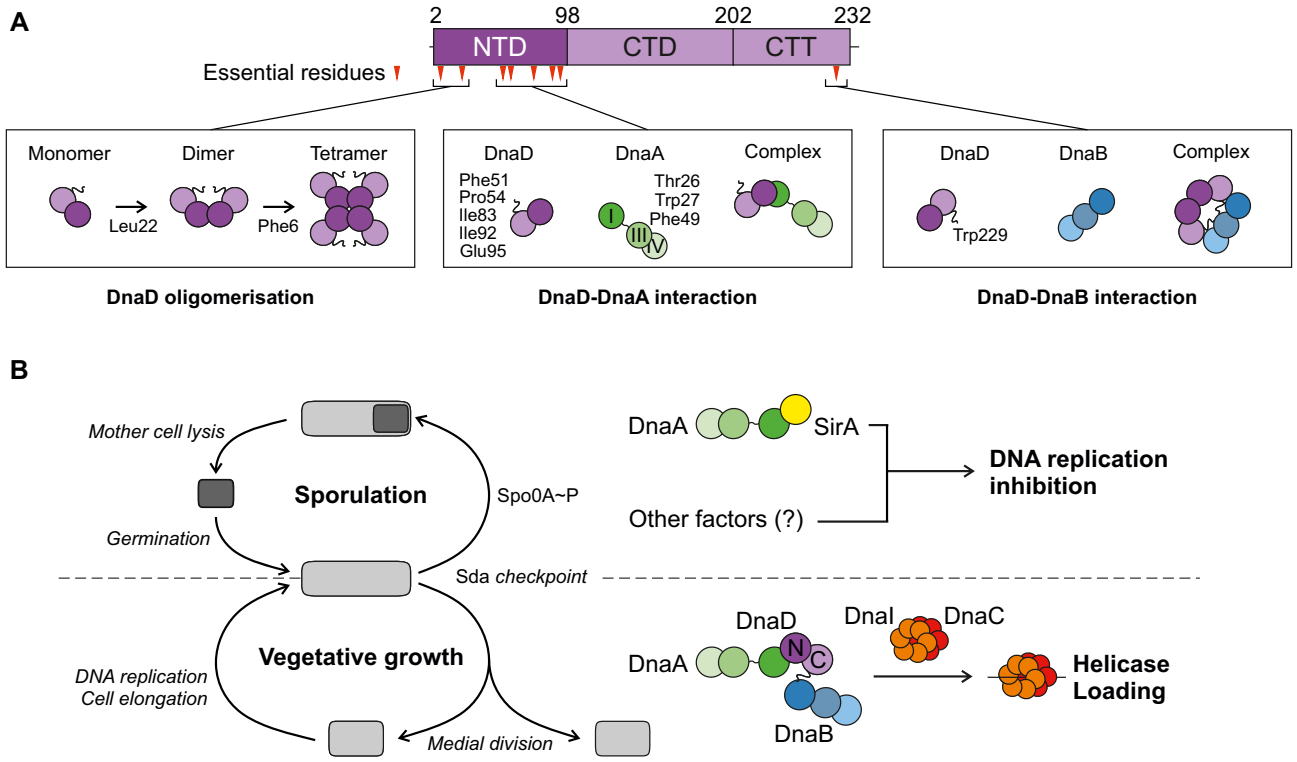

Figure 8. DnaD activities and interactions during DNA replication initiation at *oriC*. (**A**) The DnaD functional analysis identified key residues that regulate DnaD oligomerization and interactions with DnaA and DnaB. Essential residues are mapped as red triangles onto DnaD primary structure schematics with amino acid boundaries indicated. (**B**) Proposed model for the regulation of helicase loading by SirA during *B. subtilis* sporulation or by DnaD during vegetative growth. During sporulation, DnaA can interact with SirA and is depleted from the origin of replication, which leads to growth inhibition. During vegetative growth, DnaA interacts with DnaD, which in turns recruits DnaB and leads to loading of the helicase complex DnaI-DnaC; this promotes DNA replication initiation.

(Figure 5). Taken together, we propose that the essential role of the $DnaA^{DI}$–$DnaD^{NTD}$ interaction is to recruit DnaD to the replication origin.

While the DnaD alanine scan successfully pinpointed multiple protein:protein interactions, it was noteworthy that residues required for DNA binding were not identified. Previous studies established that the $DnaD^{CTD}$/$DnaD^{CTT}$ contribute to DNA binding (48,93), as well as modifying the writhe of the DNA double helix (94,95). Thus, an understanding of the role DNA binding plays for DnaD during replication initiation remains unclear.

Regulation of DNA synthesis in bacteria is mainly achieved at the stage of initiation (12). Understanding the molecular mechanisms of DNA replication initiation allows an appreciation for how extrinsic regulatory factors might modulate the pathway. This was the case here for the developmental regulator SirA, which targets the essential $DnaA^{DI}$:$DnaD^{NTD}$ interface to inhibit further rounds of DNA synthesis (Figure 7). The SirA regulatory mechanism appears crucial to achieve rapid depletion of DnaD from *oriC* during the onset of sporulation (Figure 6C-D). There appears to be a logic for *B. subtilis* regulating helicase loading at *oriC* during sporulation via SirA, as this mechanism would not perturb the interaction of DnaD with the replication restart primosome (93) required to ensure completion of genome replication (Supplementary Figure S15). The observation that DnaD and DnaA are eventually depleted from the chromosome origin in the absence of SirA indicates that other inhibitory systems are also present during sporulation, consistent with previous studies (96).

Lastly, homologs of *dnaD* are present in the majority of *Firmicutes,* including several clinically relevant human pathogens such as *Staphylococcus, Streptococcus, Enterococcus* and *Listeria* (42), and conservation of essential residues in DnaD homologs suggests that these activities are analogous (Supplementary Figure S16). Moreover, replication of *S. aureus* multiresistant plasmids have been shown to require an initiation protein with structural homology to DnaD (97). The multiple essential activities of DnaD, combined with the appreciation that helicase recruitment and loading mechanisms in bacteria and eukaryotes are distinct, indicates that DnaD homologs are attractive targets for antibacterial drug development.

DATA AVAILABILITY

All plasmids and strains are available upon request. Microscopy data reported in this paper will be shared upon request. All original code to generate the QuickChange program has been deposited at Zenodo and is publicly available as of the date of publication. The DOI of the software is https://doi.org/10.5281/zenodo.5541537.

SUPPLEMENTARY DATA

Supplementary Data are available at NAR Online.

ACKNOWLEDGEMENTS

SEC-MALS experiments were performed by Dr Andrew Leech at the Molecular Interaction laboratory as a service from the University of York.
Author contributions: C.W., D.S., S.F., S.P., E.M., P.S., A.I., H.M. contributed to the conception/design of the work. C.W., D.S., S.F., S.P., H.M. generated results presented in the manuscript. C.W., D.S., S.F., S.P. created figures. C.W. and H.M. wrote the manuscript. C.W., H.M., D.S., S.P., P.S., A.I. edited the manuscript.

FUNDING

Wellcome Trust Senior Research Fellowship [204985/Z/16/Z to H.M.]; Biotechnology and Biological Sciences Research Council [BB/P018432/1]; Queen Mary Startup funds (to A.I.); Biotechnology and Biological Sciences Research Council [BB/R013357/1 to P.S.]; Research Excellence Academy Studentship from the Faculty of Medical Sciences at Newcastle University (to D.S.); E.M. was supported by Erasmus+. Funding for open access charge: Newcastle University.
Conflict of interest statement. None declared.

REFERENCES

1. Bleichert,F., Botchan,M.R. and Berger,J.M. (2017) Mechanisms for initiating cellular DNA replication. *Science*, **355**, eaah6317.
2. Bell,S.P. and Kaguni,J.M. (2013) Helicase loading at chromosomal origins of replication. *Cold Spring Harb. Perspect. Biol.*, **5**, a010124.
3. Bramhill,D. and Kornberg,A. (1988) Duplex opening by DnaA protein at novel sequences in initiation of replication at the origin of the *e. coli* chromosome. *Cell*, **52**, 743–755.
4. Funnell,B.E., Baker,T.A. and Kornberg,A. (1987) *In vitro* assembly of a prepriming complex at the origin of the *escherichiacoli* chromosome. *J. Biol. Chem.*, **262**, 10327–10334.
5. Douglas,M.E., Ali,F.A., Costa,A. and Diffley,J.F.X. (2018) The mechanism of eukaryotic CMG helicase activation. *Nature*, **555**, 265–268.
6. Yeeles,J.T., Deegan,T.D., Janska,A., Early,A. and Diffley,J.F. (2015) Regulated eukaryotic DNA replication origin firing with purified proteins. *Nature*, **519**, 431–435.
7. Kaguni,J.M. (2018) The macromolecular machines that duplicate the *Escherichiacoli* chromosome as targets for drug discovery. *Antibiotics (Basel)*, **7**, 23.
8. van Eijk,E., Wittekoek,B., Kuijper,E.J. and Smits,W.K. (2017) DNA replication proteins as potential targets for antimicrobials in drug-resistant bacterial pathogens. *J. Antimicrob. Chemother.*, **72**, 1275–1284.
9. Robinson,A., Causer,R.J. and Dixon,N.E. (2012) Architecture and conservation of the bacterial DNA replication machinery, an underexploited drug target. *Curr. Drug Targets*, **13**, 352–372.
10. Hayashi,C., Miyazaki,E., Ozaki,S., Abe,Y. and Katayama,T. (2020) DnaB helicase is recruited to the replication initiation complex via binding of DnaA domain I to the lateral surface of the DnaB N-terminal domain. *J. Biol. Chem.*, **295**, 11131–11143.
11. Arias-Palomo,E., Puri,N., O'Shea Murray,V.L., Yan,Q. and Berger,J.M. (2019) Physical basis for the loading of a bacterial replicative helicase onto DNA. *Mol. Cell*, **74**, 173–184.
12. Jameson,K.H. and Wilkinson,A.J. (2017) Control of initiation of DNA replication in *Bacillussubtilis* and *Escherichiacoli*. *Genes*, **8**, 22.
13. Leonard,A.C. and Grimwade,J.E. (2015) The orisome: structure and function. *Front Microbiol*, **6**, 545.
14. Katayama,T., Ozaki,S., Keyamura,K. and Fujimitsu,K. (2010) Regulation of the replication cycle: conserved and diverse regulatory systems for DnaA and *oriC*. *Nat. Rev. Neurol.*, **8**, 163–170.
15. Messer,W., Blaesing,F., Majka,J., Nardmann,J., Schaper,S., Schmidt,A., Seitz,H., Speck,C., Tungler,D., Wegrzyn,G. *et al.* (1999) Functional domains of DnaA proteins. *Biochimie*, **81**, 819–825.
16. Fujikawa,N., Kurumizaka,H., Nureki,O., Terada,T., Shirouzu,M., Katayama,T. and Yokoyama,S. (2003) Structural basis of replication origin recognition by the DnaA protein. *Nucleic Acids Res.*, **31**, 2077–2086.
17. Fuller,R.S., Funnell,B.E. and Kornberg,A. (1984) The DnaA protein complex with the *E. coli* chromosomal replication origin (*oriC*) and other DNA sites. *Cell*, **38**, 889–900.
18. Roth,A. and Messer,W. (1995) The DNA binding domain of the initiator protein dnaA. *EMBO J.*, **14**, 2106–2111.
19. Schaper,S. and Messer,W. (1997) Prediction of the structure of the replication initiator protein dnaA. *Proteins*, **28**, 1–9.
20. Erzberger,J.P., Mott,M.L. and Berger,J.M. (2006) Structural basis for ATP-dependent DnaA assembly and replication-origin remodeling. *Nat. Struct. Mol. Biol.*, **13**, 676–683.
21. Erzberger,J.P., Pirruccello,M.M. and Berger,J.M. (2002) The structure of bacterial dnaa: implications for general mechanisms underlying DNA replication initiation. *EMBO J.*, **21**, 4763–4773.
22. Duderstadt,K.E., Chuang,K. and Berger,J.M. (2011) DNA stretching by bacterial initiators promotes replication origin opening. *Nature*, **478**, 209–213.
23. Ozaki,S., Kawakami,H., Nakamura,K., Fujikawa,N., Kagawa,W., Park,S.Y., Yokoyama,S., Kurumizaka,H. and Katayama,T. (2008) A common mechanism for the ATP-DnaA-dependent formation of open complexes at the replication origin. *J. Biol. Chem.*, **283**, 8351–8362.
24. Richardson,T.T., Harran,O. and Murray,H. (2016) The bacterial dnaa-trio replication origin element specifies single-stranded DNA initiator binding. *Nature*, **534**, 412–416.
25. Richardson,T.T., Stevens,D., Pelliciari,S., Harran,O., Sperlea,T. and Murray,H. (2019) Identification of a basal system for unwinding a bacterial chromosome origin. *EMBO J.*, **38**, e101649.
26. Pelliciari,S., Dong,M.J., Gao,F. and Murray,H. (2021) Evidence for a chromosome origin unwinding system broadly conserved in bacteria. *Nucleic Acids Res.*, **49**, 7525–7536.
27. Weigel,C., Schmidt,A., Seitz,H., Tungler,D., Welzeck,M. and Messer,W. (1999) The N-terminus promotes oligomerization of the *Escherichia coli* initiator protein dnaA. *Mol. Microbiol.*, **34**, 53–66.
28. Keyamura,K., Fujikawa,N., Ishida,T., Ozaki,S., Su'etsugu,M., Fujimitsu,K., Kagawa,W., Yokoyama,S., Kurumizaka,H. and Katayama,T. (2007) The interaction of DiaA and DnaA regulates the replication cycle in *e. coli* by directly promoting ATP dnaa-specific initiation complexes. *Genes Dev.*, **21**, 2083–2099.
29. Natrajan,G., Noirot-Gros,M.F., Zawilak-Pawlik,A., Kapp,U. and Terradot,L. (2009) The structure of a DnaA/HobA complex from *Helicobacter pylori* provides insight into regulation of DNA replication in bacteria. *Proc. Natl. Acad. Sci. U.S.A.*, **106**, 21115–21120.
30. Chodavarapu,S., Felczak,M.M., Yaniv,J.R. and Kaguni,J.M. (2008) *Escherichia coli* DnaA interacts with HU in initiation at the *E. coli* replication origin. *Mol. Microbiol.*, **67**, 781–792.
31. Chodavarapu,S., Gomez,R., Vicente,M. and Kaguni,J.M. (2008) *Escherichia coli* dps interacts with DnaA protein to impede initiation: a model of adaptive mutation. *Mol. Microbiol.*, **67**, 1331–1346.
32. Jameson,K.H., Rostami,N., Fogg,M.J., Turkenburg,J.P., Grahl,A., Murray,H. and Wilkinson,A.J. (2014) Structure and interactions of the *Bacillus subtilis* sporulation inhibitor of DNA replication, SirA, with domain i of dnaA. *Mol. Microbiol.*, **93**, 975–991.
33. Rahn-Lee,L., Merrikh,H., Grossman,A.D. and Losick,R. (2011) The sporulation protein SirA inhibits the binding of DnaA to the origin of replication by contacting a patch of clustered amino acids. *J. Bacteriol.*, **193**, 1302–1307.
34. Abe,Y., Jo,T., Matsuda,Y., Matsunaga,C., Katayama,T. and Ueda,T. (2007) Structure and function of DnaA N-terminal domains: specific sites and mechanisms in inter-DnaA interaction and in DnaB helicase loading on *oriC*. *J. Biol. Chem.*, **282**, 17816–17827.
35. Sutton,M.D., Carr,K.M., Vicente,M. and Kaguni,J.M. (1998) *Escherichia coli* DnaA protein. The N-terminal domain and loading of DnaB helicase at the *E. coli* chromosomal origin. *J. Biol. Chem.*, **273**, 34255–34262.

36. Mott,M.L., Erzberger,J.P., Coons,M.M. and Berger,J.M. (2008) Structural synergy and molecular crosstalk between bacterial helicase loaders and replication initiators. *Cell*, **135**, 623–634.
37. Matthews,L.A. and Simmons,L.A. (2018) Cryptic protein interactions regulate DNA replication initiation. *Mol. Microbiol.*, **111**, 118–130.
38. Smits,W.K., Goranov,A.I. and Grossman,A.D. (2010) Ordered association of helicase loader proteins with the *Bacillus subtilis* origin of replication *in vivo*. *Mol. Microbiol.*, **75**, 452–461.
39. Keyamura,K., Abe,Y., Higashi,M., Ueda,T. and Katayama,T. (2009) DiaA dynamics are coupled with changes in initial origin complexes leading to helicase loading. *J. Biol. Chem.*, **284**, 25038–25050.
40. Martin,E., Williams,H.E.L., Pitoulias,M., Stevens,D., Winterhalter,C., Craggs,T.D., Murray,H., Searle,M.S. and Soultanas,P. (2019) DNA replication initiation in *Bacillus subtilis*: structural and functional characterization of the essential DnaA-DnaD interaction. *Nucleic. Acids. Res.*, **47**, 2101–2112.
41. Seitz,H., Weigel,C. and Messer,W. (2000) The interaction domains of the DnaA and DnaB replication proteins of *Escherichia coli*. *Mol. Microbiol.*, **37**, 1270–1279.
42. Briggs,G.S., Smits,W.K. and Soultanas,P. (2012) Chromosomal replication initiation machinery of low-G+C-content firmicutes. *J. Bacteriol.*, **194**, 5162–5170.
43. Marston,F.Y., Grainger,W.H., Smits,W.K., Hopcroft,N.H., Green,M., Hounslow,A.M., Grossman,A.D., Craven,C.J. and Soultanas,P. (2010) When simple sequence comparison fails: the cryptic case of the shared domains of the bacterial replication initiation proteins DnaB and dnaD. *Nucleic Acids Res.*, **38**, 6930–6942.
44. Bruand,C., Velten,M., McGovern,S., Marsin,S., Serena,C., Ehrlich,S.D. and Polard,P. (2005) Functional interplay between the *Bacillus subtilis* DnaD and DnaB proteins essential for initiation and re-initiation of DNA replication. *Mol. Microbiol.*, **55**, 1138–1150.
45. Smits,W.K., Merrikh,H., Bonilla,C.Y. and Grossman,A.D. (2011) Primosomal proteins DnaD and DnaB are recruited to chromosomal regions bound by DnaA in *Bacillus subtilis*. *J. Bacteriol.*, **193**, 640–648.
46. Rokop,M.E. and Grossman,A.D. (2009) Intragenic and extragenic suppressors of temperature sensitive mutations in the replication initiation genes *dnaD* and *dnaB* of *Bacillus subtilis*. *PLoS One*, **4**, e6774.
47. Schneider,S., Zhang,W., Soultanas,P. and Paoli,M. (2008) Structure of the N-terminal oligomerization domain of DnaD reveals a unique tetramerization motif and provides insights into scaffold formation. *J. Mol. Biol.*, **376**, 1237–1250.
48. Carneiro,M.J., Zhang,W., Ioannou,C., Scott,D.J., Allen,S., Roberts,C.J. and Soultanas,P. (2006) The DNA-remodelling activity of DnaD is the sum of oligomerization and DNA-binding activities on separate domains. *Mol. Microbiol.*, **60**, 917–924.
49. Anagnostopoulos,C. and Spizizen,J. (1961) Requirements for transformation in *Bacillus subtilis*. *J. Bacteriol.*, **81**, 741–746.
50. Hamoen,L.W., Smits,W.K., de Jong,A., Holsappel,S. and Kuipers,O.P. (2002) Improving the predictive value of the competence transcription factor (ComK) binding site in *Bacillus subtilis* using a genomic approach. *Nucleic. Acids. Res.*, **30**, 5517–5528.
51. Wagner,J.K., Marquis,K.A. and Rudner,D.Z. (2009) SirA enforces diploidy by inhibiting the replication initiator DnaA during spore formation in *Bacillus subtilis*. *Mol. Microbiol.*, **73**, 963–974.
52. Daber,R. and Lewis,M. (2009) Towards evolving a better repressor. *Protein Eng. Des. Sel.*, **22**, 673–683.
53. Gatti-Lafranconi,P., Dijkman,W.P., Devenish,S.R. and Hollfelder,F. (2013) A single mutation in the core domain of the lac repressor reduces leakiness. *Microb. Cell Fact.*, **12**, 67.
54. Griffith,K.L. and Grossman,A.D. (2008) Inducible protein degradation in *Bacillus subtilis* using heterologous peptide tags and adaptor proteins to target substrates to the protease ClpXP. *Mol. Microbiol.*, **70**, 1012–1025.
55. Hanahan,D., Jessee,J. and Bloom,F.R. (1991) Plasmid transformation of *Escherichia coli* and other bacteria. *Methods Enzymol.*, **204**, 63–113.
56. Taylor,R.G., Walker,D.C. and McInnes,R.R. (1993) *E. coli* host strains significantly affect the quality of small scale plasmid DNA preparations used for sequencing. *Nucleic Acids Res.*, **21**, 1677–1678.
57. Li,C., Wen,A., Shen,B., Lu,J., Huang,Y. and Chang,Y. (2011) FastCloning: a highly simplified, purification-free, sequence- and ligation-independent PCR cloning method. *BMC Biotechnol.*, **11**, 92.
58. Liu,H. and Naismith,J.H. (2008) An efficient one-step site-directed deletion, insertion, single and multiple-site plasmid mutagenesis protocol. *BMC Biotechnol.*, **8**, 91.
59. Winterhalter,C. and Murray,H. (2021) Automated quickchange program. *Zenodo*, https://doi.org/10.5281/zenodo.5541537.
60. Sterlini,J.M. and Mandelstam,J. (1969) Committment to sporulation in *Bacillus subtilis* and its relationship to the development of actinomycin resistance. *Biochem. J.*, **113**, 29–37.
61. Partridge,S.R. and Errington,J. (1993) The importance of morphological events and intercellular interactions in the regulation of prespore-specific gene expression during sporulation in *bacillussubtilis*. *Mol. Microbiol.*, **8**, 945–955.
62. Schindelin,J., Arganda-Carreras,I., Frise,E., Kaynig,V., Longair,M., Pietzsch,T., Preibisch,S., Rueden,C., Saalfeld,S., Schmid,B. *et al.* (2012) Fiji: an open-source platform for biological-image analysis. *Nat. Methods*, **9**, 676–682.
63. Tinevez,J.Y., Perry,N., Schindelin,J., Hoopes,G.M., Reynolds,G.D., Laplantine,E., Bednarek,S.Y., Shorte,S.L. and Eliceiri,K.W. (2017) TrackMate: an open and extensible platform for single-particle tracking. *Methods*, **115**, 80–90.
64. Delano,W.L. (2002) In: *The PyMOL Molecular Graphics System*. Delano Scientific, San Carlos.
65. Frey,S. and Gorlich,D. (2014) Purification of protein complexes of defined subunit stoichiometry using a set of orthogonal, tag-cleaving proteases. *J. Chromatogr. A*, **1337**, 106–115.
66. Sievers,F., Wilm,A., Dineen,D., Gibson,T.J., Karplus,K., Li,W., Lopez,R., McWilliam,H., Remmert,M., Soding,J. *et al.* (2011) Fast, scalable generation of high-quality protein multiple sequence alignments using clustal omega. *Mol. Syst. Biol.*, **7**, 539.
67. Fisher,G.L., Pastrana,C.L., Higman,V.A., Koh,A., Taylor,J.A., Butterer,A., Craggs,T., Sobott,F., Murray,H., Crump,M.P. *et al.* (2017) The structural basis for dynamic DNA binding and bridging interactions which condense the bacterial centromere. *Elife*, **6**, e28086.
68. Chaudhuri,R.R., Allen,A.G., Owen,P.J., Shalom,G., Stone,K., Harrison,M., Burgis,T.A., Lockyer,M., Garcia-Lara,J., Foster,S.J. *et al.* (2009) Comprehensive identification of essential *Staphylococcus aureus* genes using transposon-mediated differential hybridisation (TMDH). *BMC Genomics*, **10**, 291.
69. Liu,X., Gallay,C., Kjos,M., Domenech,A., Slager,J., van Kessel,S.P., Knoops,K., Sorg,R.A., Zhang,J.R. and Veening,J.W. (2017) High-throughput CRISPRi phenotyping identifies new essential genes in *Streptococcus pneumoniae*. *Mol. Syst. Biol.*, **13**, 931.
70. Kobayashi,K., Ehrlich,S.D., Albertini,A., Amati,G., Andersen,K.K., Arnaud,M., Asai,K., Ashikaga,S., Aymerich,S., Bessieres,P. *et al.* (2003) Essential *Bacillus subtilis* genes. *Proc. Natl. Acad. Sci. U.S.A.*, **100**, 4678–4683.
71. Collier,C., Machon,C., Briggs,G.S., Smits,W.K. and Soultanas,P. (2012) Untwisting of the DNA helix stimulates the endonuclease activity of *Bacillus subtilis* nth at AP sites. *Nucleic Acids Res.*, **40**, 739–750.
72. Ishikawa,S., Ogura,Y., Yoshimura,M., Okumura,H., Cho,E., Kawai,Y., Kurokawa,K., Oshima,T. and Ogasawara,N. (2007) Distribution of stable dnaa-binding sites on the *Bacillus subtilis* genome detected using a modified chip-chip method. *DNA Res.*, **14**, 155–168.
73. Zhang,W., Carneiro,M.J., Turner,I.J., Allen,S., Roberts,C.J. and Soultanas,P. (2005) The *Bacillus subtilis* DnaD and DnaB proteins exhibit different DNA remodelling activities. *J. Mol. Biol.*, **351**, 66–75.
74. Marsin,S., McGovern,S., Ehrlich,S.D., Bruand,C. and Polard,P. (2001) Early steps of *Bacillus subtilis* primosome assembly. *J. Biol. Chem.*, **276**, 45818–45825.
75. Webb,C.D., Teleman,A., Gordon,S., Straight,A., Belmont,A., Lin,D.C.-H., Grossman,A.D., Wright,A. and Losick,R. (1997) Bipolar localization of the replication origin regions of chromosomes in vegetative and sporulating cells of *B. subtilis*. *Cell*, **88**, 667–674.
76. Imai,Y., Ogasawara,N., Ishigo-Oka,D., Kadoya,R., Daito,T. and Moriya,S. (2000) Subcellular localization of Dna-initiation proteins of *Bacillus subtilis*: evidence that chromosome replication begins at either edge of the nucleoids. *Mol. Microbiol.*, **36**, 1037–1048.

77. Kohler,P. and Marahiel,M.A. (1997) Association of the histone-like protein HBsu with the nucleoid of *Bacillus subtilis*. *J. Bacteriol.*, **179**, 2060–2064.
78. Wang,X., Montero Llopis,P. and Rudner,D.Z. (2014) *Bacillus subtilis* chromosome organization oscillates between two distinct patterns. *Proc. Natl. Acad. Sci. U. S. A.*, **111**, 12877–12882.
79. Karimova,G., Pidoux,J., Ullmann,A. and Ladant,D. (1998) A bacterial two-hybrid system based on a reconstituted signal transduction pathway. *Proc. Natl. Acad. Sci. U. S. A.*, **95**, 5752–5756.
80. Hagel,L. (2001) Gel-filtration chromatography. *Curr. Protoc. Mol. Biol.*, https://doi.org/10.1002/0471142727.mb1009s44.
81. Wyatt,P.J. (1993) Light scattering and the absolute characterization of macromolecules. *Anal. Chim. Acta*, **272**, 1–40.
82. Andrup,L., Atlung,T., Ogasawara,N., Yoshikawa,H. and Hansen,F.G. (1988) Interaction of the *Bacillus subtilis* dnaa-like protein with the *Escherichia coli* DnaA protein. *J. Bacteriol.*, **170**, 1333–1338.
83. Krause,M. and Messer,W. (1999) DnaA proteins of *Escherichia coli* and *Bacillus subtilis*: coordinate actions with single-stranded DNA-binding protein and interspecies inhibition during open complex formation at the replication origins. *Gene*, **228**, 123–132.
84. Santos-Pereira,J.M. and Aguilera,A. (2015) R loops: new modulators of genome dynamics and function. *Nat. Rev. Genet.*, **16**, 583–597.
85. Kogoma,T. and von Meyenburg,K. (1983) The origin of replication, *oriC*, and the DnaA protein are dispensable in stable DNA replication (*sdrA*) mutants of *Escherichia coli* K-12. *EMBO J.*, **2**, 463–468.
86. Hassan,A.K., Moriya,S., Ogura,M., Tanaka,T., Kawamura,F. and Ogasawara,N. (1997) Suppression of initiation defects of chromosome replication in *Bacillus subtilis dnaA* and *oriC*-deleted mutants by integration of a plasmid replicon into the chromosomes. *J. Bacteriol.*, **179**, 2494–2502.
87. Berkmen,M.B. and Grossman,A.D. (2007) Subcellular positioning of the origin region of the *Bacillus subtilis* chromosome is independent of sequences within *oriC*, the site of replication initiation, and the replication initiator dnaA. *Mol. Microbiol.*, **63**, 150–165.
88. Breier,A.M. and Grossman,A.D. (2009) Dynamic association of the replication initiator and transcription factor DnaA with the *Bacillus subtilis* chromosome during replication stress. *J. Bacteriol.*, **191**, 486–493.
89. Errington,J. (2003) Regulation of endospore formation in *Bacillus subtilis*. *Nat. Rev. Microbiol.*, **1**, 117–126.
90. Rahn-Lee,L., Gorbatyuk,B., Skovgaard,O. and Losick,R. (2009) The conserved sporulation protein YneE inhibits DNA replication in *Bacillus subtilis*. *J. Bacteriol.*, **191**, 3736–3739.
91. Molle,V., Fujita,M., Jensen,S.T., Eichenberger,P., Gonzalez-Pastor,J.E., Liu,J.S. and Losick,R. (2003) The Spo0A regulon of *Bacillus subtilis*. *Mol. Microbiol.*, **50**, 1683–1701.
92. Su'etsugu,M. and Errington,J. (2011) The replicase sliding clamp dynamically accumulates behind progressing replication forks in *Bacillus subtilis* cells. *Mol. Cell*, **41**, 720–732.
93. Huang,Y.H., Lien,Y., Huang,C.C. and Huang,C.Y. (2016) Characterization of *Staphylococcus aureus* primosomal DnaD protein: highly conserved C-Terminal region is crucial for ssDNA and PriA helicase binding but not for DnaA protein-binding and self-tetramerization. *PLoS One*, **11**, e0157593.
94. Zhang,W., Allen,S., Roberts,C.J. and Soultanas,P. (2006) The *Bacillus subtilis* primosomal protein DnaD untwists supercoiled DNA. *J. Bacteriol.*, **188**, 5487–5493.
95. Zhang,W., Machon,C., Orta,A., Phillips,N., Roberts,C.J., Allen,S. and Soultanas,P. (2008) Single-molecule atomic force spectroscopy reveals that DnaD forms scaffolds and enhances duplex melting. *J. Mol. Biol.*, **377**, 706–714.
96. Boonstra,M., de Jong,I.G., Scholefield,G., Murray,H., Kuipers,O.P. and Veening,J.W. (2013) Spo0A regulates chromosome copy number during sporulation by directly binding to the origin of replication in *Bacillus subtilis*. *Mol. Microbiol.*, **87**, 925–938.
97. Schumacher,M.A., Tonthat,N.K., Kwong,S.M., Chinnam,N.B., Liu,M.A., Skurray,R.A. and Firth,N. (2014) Mechanism of staphylococcal multiresistance plasmid replication origin assembly by the RepA protein. *Proc. Natl. Acad. Sci. U.S.A.*, **111**, 9121–9126.